Performance of Topological Quantum Error Correction in the Presence of Correlated Noise

Muhammad Ahsan

August 3, 2023

Abstract

We investigate the efficacy of topological quantum error-correction in correlated noise model which permits collective coupling of all the codeword qubits to the same non-Markovian environment. In this noise model, the probability distribution over set of phase-flipped qubits, decays sub-exponentially in the size of the set and carries non-trivial likelihood of the occurring large numbers of qubits errors. We find that in the presence of noise correlation, one cannot guarantee arbitrary high computational accuracy simply by incrementing the codeword size while retaining constant noise level per qubit operation. However, if instead, per-operation qubit error probability in an n-qubits long codeword is reduced $O(\sqrt{n})$ times below the accuracy threshold, arbitrarily accurate quantum computation becomes feasible with acceptable scaling of the codeword size. Our results suggest that progressively reducing noise level in qubits and gates is as important as continuously integrating more qubits to realize scalable and reliable quantum computer.

1 Introduction

Vast literature on fault-tolerant quantum computing has convincingly established the principle effectiveness of quantum error correction [48, 50, 33, 31, 35] in combating the noise which causes qubits (and gates) fail independently due to decoherence [23]. In the independent noise model, a sizable quantum computational algorithm can be executed with arbitrarily low inaccuracy provided that noise level p, defined as failure probability per operation, is kept below certain constant accuracy threshold value i.e. $p < p_{th}$ [1, 5]. Once threshold constraint is satisfied, efficiently reducing the execution inaccuracy becomes a matter of modestly enlarging size of error-correcting codeword. For some constant $c > 0$, the execution inaccuracy $\epsilon \sim n^c(p/p_{th})^{f(n)}$ decreases exponentially in the error-correcting code overhead cost $f(n)$ defined as monotonically increasing function of n: the number of codeword qubits. Most remarkably, $f(n)$ highlights manageable overhead cost by growing no faster than the poly-logarithmic function of n and $1/\epsilon$ i.e. $O(poly(log(n/\epsilon)))$ [1]. This landmark result envisions reliable quantum computing hardware which will feature both the

(i) *scalability*: because progressively large-scale computation can be executed with acceptable scaling of the codeword qubits overhead and (ii) *fault-tolerance*: because vanishingly small inaccuracy can be achieved with fixed noise level. The entire foundation of fault-tolerant quantum computation is rooted in the following interpretation of the threshold-theorem: that the existence of constant noise threshold suffices both the scalability and fault-tolerance for independent noise model.

In this work we show that the fulfillment of threshold condition alone may not yield fault-tolerance in a more general and realistic noise model that correlates the failure of qubits (and gates) in time and space. Our conclusion is founded on the detailed simulation based performance analysis of surface error-correcting code [9] subject to correlated noise. In this noise model, all the codeword qubits jointly interact with the same non-Markovian environment [10, 34] which is not refreshed until single trial of syndrome measurement is completed. The entanglement, among codeword qubits states, enables an overall constructive interference among the temporally and spatially correlated fault-paths leading to larger number of errors in the codeword. In contrast to its independent counterpart which assigns exponentially small (in n) probability to the uncorrectable errors [1], the correlated noise significantly elevates the likelihood of more codeword qubits in error than those can be perfectly corrected by the surface code. More frequent occurrence of these many-qubit errors severely limits the sharp decline in the overall execution inaccuracy unless noise correlations are sufficiently curtailed in physical quantum device which may in turn pose complex engineering challenges [28, 4].

At this point our investigation crucially reveals that in the sub-threshold region ($p < p_{th}$), the noise level in the individual qubit is directly proportional to the accumulated failure probability of the qubit due to correlated errors in gate/measurement operation. Therefore, by tuning the metric *per-operation qubit error probability*, the strength of noise correlation can be proportionally and precisely controlled. The metric not only provides an appropriate scale to measure the magnitude of both independent and correlated noise model but also enables fair comparison of surface-code performance between the two models. Our simulations show that the attainment of arbitrarily low inaccuracy is contingent not only upon increasing the surface-code codeword size equal to that for the independent noise case, but also reducing noise level per qubit (or gate) by $O(\sqrt{n})$ where n is the number of codeword qubits.

Although our findings clearly indicate the non-compliance of correlated noise model with the standard pre-requisite of quantum fault-tolerance, these do not preclude the possibility of large-scale quantum computation if experimental efforts do not settle with constant noise level just below threshold! Considering that realistic noise in quantum hardware may have correlated character, progressively larger and reliable quantum computing device can be built if, in addition to integrating more component qubits and gates in the system, experimentalists concurrently strive to steadily lower noise levels in these components. Therefore by bringing the importance of high quality qubits to the surface, our work provides crucial design guidelines

to the experimentalist community trying to realize scalable quantum computer.

In order to systematically explicate our results, we first introduce background knowledge and relevant prior work to the unfamiliar audience in Section-2. Next, we summarize salient contribution of our work in Section-3. Finally, rest of the paper is organized as follows: Section-4 describes correlated noise model while Section-5 provides an overview of surface error-correcting code. The simulation results are provided in Section-6 , discussed in Section-7. The gist of this work is compiled and concluded in Section-8.

2 Contextual motivation behind this work

2.1 Noise and fault-tolerance in quantum computing

In real-life applications, the quantum speedup comes from growing and sustaining a fragile Hilbert space spanned by the superposition of qubits states. During the execution of algorithm on intrinsically noisy hardware, the quantum mechanical orientation of superposition state decays over time and eventually reduces to statistical representation of classical information bits [23]. This process is termed decoherence and it prohibits scalable quantum computation unless noise accumulation is confined to acceptable limits [48]. In the paradigm of *independent* noise [42], the decoherence of a given qubit state is assumed completely oblivious to its quantum mechanical correlations (e.g. entanglement) with other qubits in the system and its past interaction with the unwanted surroundings called *environment*. Fortunately, this type of decoherence can be treated by encoding each *logical* qubit into several constituent qubits using suitable quantum error correcting codes and repeatedly purifying its state from errors arising from noisy operations [36]. Using multiple layers of encoding [33, 12] or increasing the size of error correcting code [45, 31], arbitrary gain in fault-tolerance is attainable, provided that the magnitude of independent noise (failure probability per operation) is below constant threshold (a.k.a accuracy threshold) value [1]. The information recovering ability of quantum error correction has been successfully validated [15] using commercially available small-scale quantum processors (e.g. IBM 5 or 16 qubits processor). It should be noted that once qubit is encoded, fault-tolerance quantum computation proceeds by applying gate(s) directly on the encoded qubit. Such a gate is called encoded or logical gate.

The threshold value indirectly quantifies noise margin in quantum computing device; should the noise level in component qubits (and gates), exceeds the threshold, errors accumulate faster than they are corrected [48]. These errors enact undetectable unwanted logical gate on the encoded qubit, irrevocably altering its state. Consequently, the probability of recovering the uncorrupted state of encoded qubit can no longer acquire value arbitrarily close to unity. On contrary, it will approach zero [36] with the increase in encoding layers or code-distance, defeating the very purpose of fault-tolerance. Hence the error correcting code with higher threshold

value, can tolerate higher noise levels by eliminating more combinations of errors in the qubits and gates. Such codes have historically been considered the holy grail of fault-tolerant quantum computing; their quest [33, 6] was initiated soon after the inception of pioneering work on quantum error correction [48]. Among broad classes of different techniques proposed and investigated for high threshold error correction [33, 6, 31, 45], the surface code [9] has specifically received considerably higher attention. By virtue of its simpler error decoding scheme, surface code decomposes complex decoherence patterns into orthogonal sets of errors distribution that can efficiently decoded and corrected along time and space axes with high accuracy. The procedure for extracting error syndrome comprises quantum gates which translate into spatially local physical operations in the quantum hardware. By obviating inherently noisy and resource consuming long-distance gates, the error correction procedure manifests elegant performance through greater efficiency and reliability. Vast literature on the fault-tolerance analysis of surface code can be found in Refs [20, 18, 51, 53, 14] and briefly reviewed in Section-5.

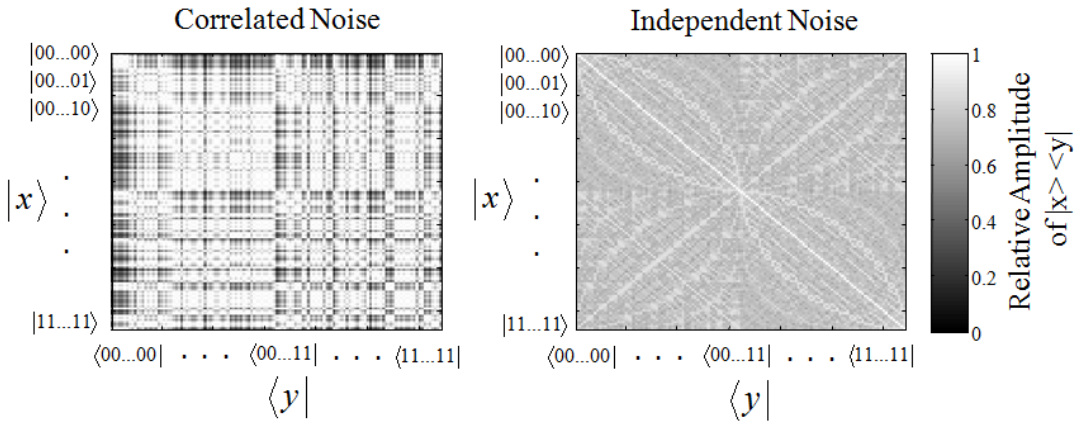

Figure 1: The gray-scale map of a 13-qubits surface code density matrix $\rho(t)$, colors each $|x\rangle\langle y|$ coherence according to its noise reduced amplitude. The noise strength $L(t, d_{l,m})$ (defined in Section-4) is set to 0.04 for both the noise models.

2.2 Brief review of correlated noise

In a realistic quantum hardware the architectural constraints inevitably house block of qubits in the same environment and invalidate the independent noise assumption [16]. For example, the qubits mapped to the linear array of trapped-ions will couple to the common vibrational modes of the chain of ions [30]. The quantum dot qubits are

localized in the same lattice along with sharing same phonon bath [40], and single resonator connects multiple qubits in the superconductor quantum computer [21]. Naturally, the perturbation induced in the target qubits by the imperfect gates, may propagate to the neighboring qubits and produce spatial correlation in noise. Likewise, when a qubit interacts with the same apparatus (e.g. an ion excited by same laser) multiple times for the sequence of gates operations, the errors may also correlate with each other in time due to the inherent memory of the environment [29]. These spatial-temporal noise correlations cause certain qubits states disappear more prominently than the others. For example, when multiple qubits collectively interact with the same environment [16, 56], their mutual pairwise-entanglement causes higher attenuation of the non-diagonal elements of the density matrix [42] than that in case of each qubit interacting with the different environment. Therefore, the states containing higher disparity between the number of 1's or 0's become more vulnerable to the spatially correlated noise. Similarly, for highly entangled states, temporal correlations allow errors to accumulate faster [41] than they are corrected, unless some of these are canceled by flipping qubit state between $|0\rangle$ and $|1\rangle$ periodically [57, 47].

In addition to the incongruent decoherence of different qubits state, the capricious nature of environment may also characterize the correlated noise. Its usual role of sinking the leaked qubit information may suddenly reverse to further complicate the noise process. This role reversal may recover a component of lost information from environment, returns it to the qubit and partially revive the coherence [22] at some point during the joint evolution of qubit and its environment. Such flickering noise behavior not only complicates the accurate book keeping of the probability distribution of errors but also marks variegated information loss across qubits Hilbert space [32]. This problem particularly accentuates for the long-lasting joint evolution of qubit-environment wave-function based on the *memory span* of the environment, typical of several quantum devices technologies [38, 52, 17, 25, 8]. Longer memory span unearths the *non-Markovian* nature environment that increases the covariance (or correlation) of the failure rates of the sequential noisy operations. Hence both the qubits mutual entanglement and the environment memory contribute to the complex nature of correlated noise. Since noise correlations tend to leave *heterogeneous* imprints of amplitude decay in the qubits Hilbert space [32]; the noise-reduced amplitudes of the density matrix elements depict substantially higher variance in a typical correlated model when compared with its independent counterpart as illustrated by an example in Figure-1. This varying amplitude loss across the Hibert space features one of the defining attributes of correlated noise and seems to undermine the efficacy of fault-tolerant techniques proposed for the independent noise model.

The design of error-correcting code depends upon the probability distribution of errors which is inversely proportional to the *fidelity* of the encoded qubits state. The fidelity metric which finds the *closeness* between the noiseless and the noisy qubits state, is calculated by averaging the amplitude decay over the entire density matrix. Unfortunately, calculation of fidelity becomes intractable as the size of Hilbert space

grows exponentially in the number of qubits. Alternatively, a conservative approximation of errors probability distribution is efficiently obtained by considering only the worst case amplitude decay which maps to (lowest fidelity) darkest regions in Figure-1. By lending itself to the worst-case analysis, the correlated model gathers non-trivial likelihood of uncorrectable errors (*many-qubits* errors) which remains exponentially small otherwise [23]. For this reason, correlated noise is often cited as one of strongest impediment of achieving large-scale quantum computation [4, 26, 27] in a realistic noisy hardware. However, because the conclusions based on the worst-case behavior often yield pessimistic performance estimates, more sophisticated theoretical and experimental analysis techniques are required for the precise quantification of performance degradation. Hence, even though the existence of correlated noise has been established through environment engineering based proof-of-concept experiments [10, 34, 38, 37, 13, 8], the detailed characterization and profound implications on fault-tolerant quantum computation have remained an unexplored frontier and deserve careful investigation.

2.3 Prior work on correlated noise

Prior studies on correlated noise fall into the broader spheres of non-Markovian and adversarial noise in and were conducted in framework of qualitative performance analysis. The adversarial noise models [28] hypothesize specific correlations among qubits errors which exploit inherent limitations of the fault tolerant protocols. The encoded Hilbert space is transformed in a way which complicates the detection of errors and recovery of original logical state, for example, by changing the amplitude of individual codewords in the superposition in proportion to their Hamming weights [43, 7]. Adversarial models are often leveraged by skeptics of quantum computation to posit intricate ways in which the Hilbert space may irreversibly decohere [28, 4]. However such models are comparatively premature as their foundation in a realistic quantum hardware seeks credible justification [49].

In contrast, the non-Markovian models [22, 11, 10, 34] portray more quantum mechanical picture of correlated noise: a time-dependent Hamiltonian describing interaction between system and the environment [54, 5]. The joint evolution of the system-environment wave-function generates entanglement between the two subsystems which acts a source of *memorizing* the noise-induced changes in system state over time and space. The collapse of wave-function projects accumulated noise onto spatially and temporally correlated errors in the system qubits. By upper bounding the norm of evolving Hamiltonian, accuracy thresholds for various settings of system-environment coupling have been established [2, 44, 5, 54]. The non-Markovian models generally provide adequate holistic overview of correlated noise process. Unfortunately, the Hamiltonian descriptions in the prior studies tend to abstract deeper insights into the transformation of system Hilbert space which can aid in engineering error correcting codes which are resistant to noise correlation.

It is important to note that the aforementioned accuracy threshold results con-

sider system-environment Hamiltonian models which fulfill *local noise condition*. The qubits errors herein, can interfere constructively or destructively over the memory span of the environment, yet the net *amplitude* of k faulty qubits in the error-correction circuit, declines exponentially in k. The amplitude reduces to the classical probability in a special case of local noise called independent noise. It assigns exponentially small probability to the occurrence many qubits errors (large k), without their mutual interference. On contrary, our correlated noise lowers this probability only sub-exponentially in k and accumulates non-negligible weight of many qubits errors. In this sense, the correlated noise in this study may be best characterized *non-local* in the context of prior work. We highlight the dichotomy between local and non-local noise to properly situate our work within prior studies [2, 44, 5, 54] primarily based on concatenated code fault-path counting techniques. On the other hand, the relevant surface-code literature [20, 53, 51, 14] reflects similar dichotomy viz., independent versus correlated noise. Since our work is specific to surface code, we shall purposely avoid the use of terms: local and non-local, and remain consistent with the independent and correlated noise terminology in order to dispel nomenclature confusion.

In a fault-tolerant quantum computer design, constant accuracy threshold determines noise margin of component devices and acts as canonical yardstick of reliable computation [1, 5]. While constant threshold has been shown for several non-Markovian noise models [54, 2, 44], it is often precluded by certain types of adversarial noise which permit highly correction-proof errors (e.g. synchronized or controlled-phase flips [7, 26, 27]). Although, these conflicting findings and other similar results [46] adequately explore multifaceted implications for the fault-tolerant quantum computing [49], the concrete performance evaluation of error correcting code (quantified as probability of misinterpreting the logical state of qubit after error-correction or *logical failure probability*) remains a difficult task due to the following reasons:

- Computational intractability impedes the efficient translation of the (in)fidelity of exponential size noisy Hilbert space to the probability distribution of errors in correlated model
- Noise correlations complicate the application of standard fault-path counting techniques when the probability of large number of errors is non-trivial
- It is difficult to quantitatively juxtapose correlated noise with its independent counterpart for the comparison on the same scale of noise strength
- The analysis of effective correction of adversarial error patterns, when the strength of correlated noise is below accuracy threshold (sub-threshold region), has thus far remain elusive

Our study makes humble attempt to fill in these crucial gaps and aims at advancing ongoing investigations on this vast and complex topic.

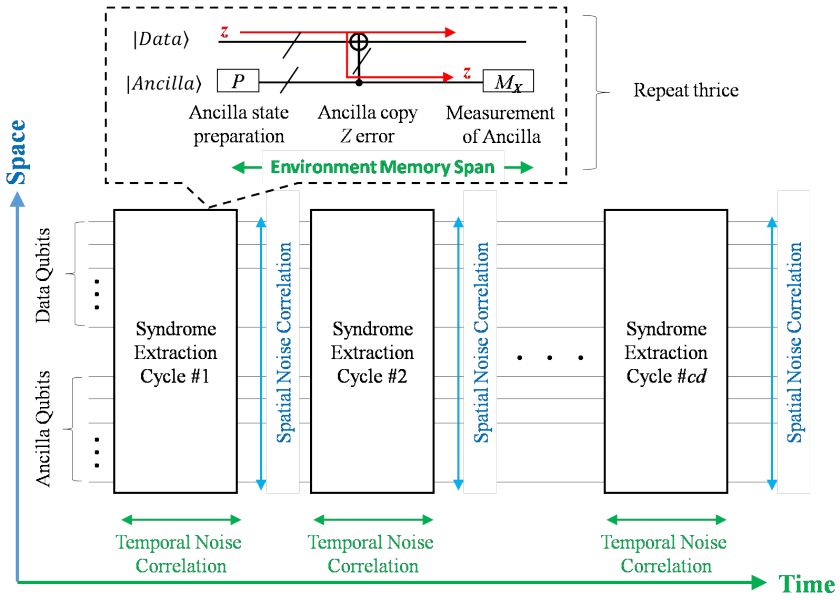

Figure 2: (Color online) Block diagram of surface code error correction consisting of cd (code distance) number of syndrome extraction cycles. Each cycle comprises three trials of syndromes measurement shown in the dotted box. The spatial noise correlations span all the qubits while the temporal correlations are confined to the duration of single syndrome measurement trial

3 Salient technical features of this work

In this work we present a realistic correlated noise model which maps to the known quantum device technologies and befits the structure of proposed error correction schemes. A computationally efficient technique is derived which translates noisy qubits density matrix into probability distribution of errors. We adopt a quantitative approach by statistically comparing together the logical failure probability for correlated and independent noise models using single comparative scale: *per-operation qubit error probability*. Being applicable to both noise models, the scale can be experimentally obtain by familiar quantum state tomography techniques [58, 39]. Using this scale, we explore the noise sub-threshold region to evaluate the performance of topology-centric quantum error correction subject to the noise which exploits the topological correlation among the qubits. In particular, the paper technically contributes along four specific directions:

- Neat picture of a parameterizable spatial-temporal correlated noise model which
    1. presents quantum circuit based more intuitive description of correlated noise
    2. conforms to the conventional understanding of the decoherence process
    3. provides single parameter knob to precisely control the strength of noise correlation in the sub-threshold region
    4. enables us to *zoom in* the system density matrix and to selectively observe the element-wise amplitude decay of non-diagonal terms
- Detailed performance analysis of the error correction including the fidelity of ancillary (or ancilla) qubits state used in extracting syndromes of correlated errors
- Insightful performance comparison of error correcting code between correlated and independent noise models on the same scale of noise strength in the sub-threshold region
- Efficient and accurate performance simulation of complete error correction protocol processing the Hilbert space of up to 1000 qubits

Our spatial-temporal correlated noise model is inspired by the recent experimental advances in general purpose trapped-ion quantum hardware [30]. Its basic building block contains several ions whose spins (system) jointly couple to the common phonon field (environment) which facilitates local execution of multi-qubits gates. The spatially correlated decoherence arises from the collective entanglement of ionic qubits to the field modes and is quantified as average amplitude decay of the non-diagonal terms of the traced-out system density matrix. Moreover, the experimentally established non-Markovian nature of the phonon field [11] introduces memory into the

environment and accounts for the temporal noise correlation. The overall infidelity is described by a flat-ended, sub-exponentially decaying probability distribution curve assigning non-negligible likelihood to the occurrence of many-qubits errors in time and space.

We choose surface error-correcting code for its ability to correct appreciable combinations of many-qubits errors, high accuracy threshold and regular 2-D grid-topology conducive to hardware implementation. During error correction, although each full round (shown as rectangle in Figure-2) of syndromes extraction involves all the qubits in the codewords, the periodic discretization of errors, through the ancilla measurements, naturally limits the span of temporal noise correlation (dotted box in Figure-2). Thus when surface code is subjected to short duration non-Markovian and long-range spatially correlated noise, we find that constant accuracy threshold exists and is 3x lower than that in case of independent noise. However, in the sub-threshold region, the logical failure probability decays exponentially slower compared to the independent noise. We show that by reducing per-operation qubit error probability $\sim n^{0.5}$ times in an n-qubits long surface code, the logical failure probability becomes sufficiently small to enable scalable quantum computation.

4 Correlated Noise Model

The noise process considered in this work is of type $T2$ decoherence [23] described by the gradual disappearance of qubit superposition state contained in the non-diagonal terms (or *coherences*) of its density matrix. The process involves joint unitary evolution of the qubit and its environment which increases the orthogonality among the environment basis states over time and entangles these with the qubit coherences. When the environment is traced out, the vanishing overlap among its states is reflected as shrinking coherence amplitude in the qubit density matrix [42]. In case of multi-qubits system, the configuration of qubits-environment coupling determines the nature of noise. The qubits will independently decohere if their corresponding coupling environments are quantum mechanically uncorrelated in time and space. Otherwise, depending upon their interaction with the environment, qubits are generally subject to the correlated noise [22].

Our selection of the correlated noise model is driven by the proposals of quantum computer architectures which advocate local execution of gates in the hardware. The local gates which are naturally fast, less noisy and resource efficient, entail high degree of spatial proximity among the qubits when mapped to the quantum hardware [55, 3]. When spatial locality is increased the qubits tend to share and collectively couple to the same environment and fall victim to the spatially correlated noise. Unlike several prior studies which model such type of noise using spin-boson Hamiltonian abstraction [42], we present quantum circuit based intuitive snapshot of collective decoherence. Nevertheless, the Hamiltonian description will be leveraged to highlight the physical interpretation of our model parameters.

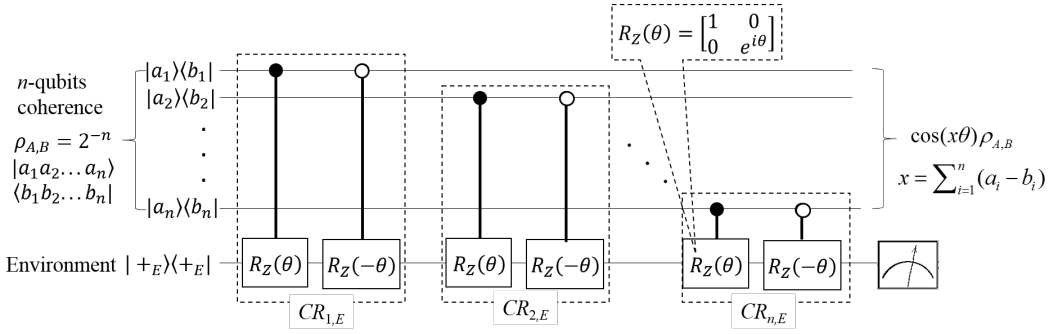

Figure 3: The circuit model description of our spatially correlated noise

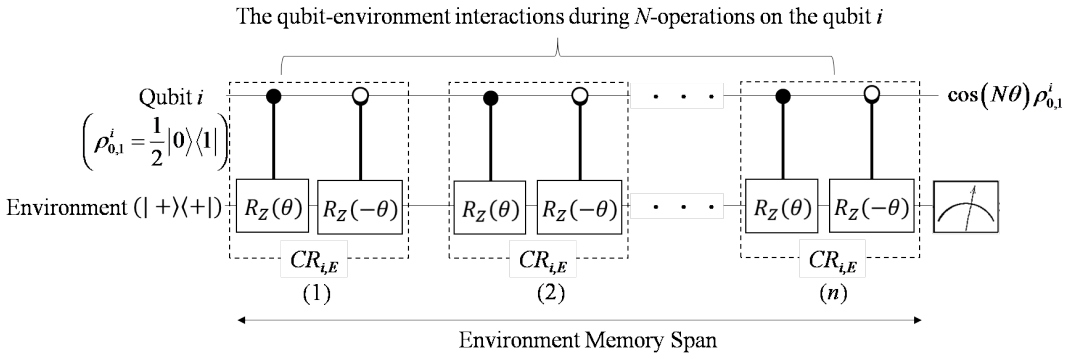

Figure 4: The circuit model description of our temporally correlated noise

4.1 Circuit model description

A quick intuition into the collective decoherence can be obtained by considering a relatively simple case of two qubits (1,2), both influenced by the same environment(E) in Figure-3. Each qubit i applies controlled-phase operation $CR_{i,E} := |0_i\rangle\langle 0_E| + e^{-i\theta}|0_i\rangle\langle 1_E| + |1_i\rangle\langle 0_E| + e^{i\theta}|1_i\rangle\langle 1_E|$ on the environment. For a single qubit decoherence, the initially uncoupled qubit and environment tensor product state $|\psi\rangle := |+_i\rangle \otimes |+_E\rangle \equiv |+_i\rangle|+_E\rangle$ (where $|+\rangle := \frac{1}{\sqrt{2}}|0\rangle + |1\rangle$) will be transformed by $CR_{i,E}$ as follows:

$$\frac{1}{\sqrt{2}}(|0_i\rangle + |1_i\rangle) \otimes \frac{1}{\sqrt{2}}(|0_E\rangle + |1_E\rangle) \xrightarrow{CR_{i,E}} \frac{1}{2}[(|0_i\rangle(|0_E\rangle + e^{-i\theta}|1_E\rangle) + |1_i\rangle(|0_E\rangle + e^{i\theta}|1_E\rangle)]$$

The amplitude of qubit coherences $\rho_{0,1} = |0\rangle\langle 1|$ in the reduced density matrix becomes the $\frac{1}{2}(\langle 0_E|0_E\rangle + e^{2i\theta}\langle 1_E|1_E\rangle) = \cos(\theta)$. By Taylor Series expansion, for small θ, $\cos(\theta) \approx 1 - \theta^2/2! \approx e^{-\theta^2/2}$ which quantifies infidelity incurred in the single qubit state (Figure-3). However, when both qubits jointly couple with the environment, the their collective decoherence depends upon the pre-existing entanglement between the two qubits. For example when both the qubits apply controlled-phase gate (with same θ) on the environment, the state $|\phi^-\rangle = \frac{1}{\sqrt{2}}(|0_1 1_2\rangle + |1_1 0_2\rangle)$ remains disentangled, while $|\phi^+\rangle = \frac{1}{\sqrt{2}}(|0_1 0_2\rangle + |1_1 1_2\rangle)$ entangles with the environment:

$$\frac{1}{\sqrt{2}}(|0_1 0_2\rangle + |1_1 1_2\rangle)\frac{1}{\sqrt{2}}(|0_E\rangle + |1_E\rangle) \xrightarrow{CR_{1,E}, CR_{2,E}}$$
$$\frac{1}{2}[(|0_1 0_2\rangle(|0_E\rangle + |1_E\rangle) + |1_1 1_2\rangle(|0_E\rangle + e^{2i\theta}|1_E\rangle)]$$

In this case the amplitude of two-qubits coherence $\rho_{00,11} = |0_1 0_2\rangle\langle 1_1 1_2|$ becomes $e^{-4\theta^2/2}$. For the general case of n-qubits system, coherence $\rho_{A,B}$ defined as $\rho_{a_1 a_2 a_3 \ldots a_n, b_1 b_2 b_3 \ldots b_n} = |a_1 a_2 a_3 \ldots a_n\rangle\langle b_1 b_2 b_3 \ldots b_n|$, the coherent state of each qubit (i.e. when $a_i = |1\rangle$ and $b_i = |0\rangle$ or vice versa) adds factor $(a_i - b_i)\theta$ to the hitherto accumulated rotation in $|+_E\rangle$. The same factor squared, reflects back into the amplitude of coherence upon tracing out the environment. Hence the aggregate rotation: $\sum_{i=1}^{n}(a_i - b_i)\theta$ contributed by all n-qubits, leaves $\rho_{A,B}$ amplitude decaying exponentially in $|\sum_{i=1}^{n}(a_i - b_i)|^2\theta^2$ same as shown in Ref[42].

A remarkable feature of this model is the neat geometric interpretation of the correlated noise shown in Figure-5. Each qubit depending upon its $|0\rangle$, $|1\rangle$ state, rotates the environment state vector: $|v_E\rangle = |+_E\rangle$ by angle $\theta/2$, $-\theta/2$ about z-axis of the Bloch sphere respectively. In case of multi-qubits system, each qubit state in the coherence contributes to the aggregate rotation in $|v_E\rangle$. The collective decoherence of $|A\rangle\langle B|$, is quantified by the projection of $|A\rangle$ rotated $|v_E\rangle$ on the $|B\rangle$ rotated $|v_E\rangle$. In an example of a two-qubits state $|\phi^-\rangle$ we see the rotation caused by one qubit is canceled by the other, resulting in no decoherence. On contrary, the state $|\phi^+\rangle$ constructively adds the two rotations which ensues quadratically enlarged decoherence.

The constructive and destructive interference among the rotations naturally amplifies decay of certain coherences while leaving others completely unchanged. The large variation in coherence decay sharply contrasts with the monotonous decline in case of the independent noise.

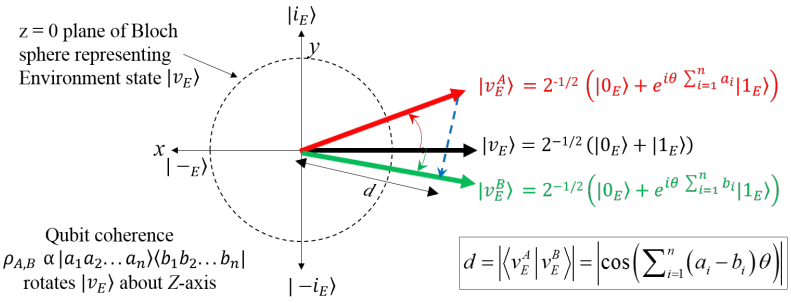

Figure 5: (Color online) Geometric interpretation of correlated decoherence. The initial environment state $|v_E\rangle$ becomes $|v_E^A\rangle$ and $|v_E^B\rangle$ and when rotated by state qubits coherence $|A\rangle$ and $|B\rangle$ respectively. The overlap between $|v_E^A\rangle$ and $|v_E^B\rangle$ is shown as projection length d. Note that $|-_E\rangle \equiv \frac{1}{\sqrt{2}}(|0\rangle - |1\rangle)$.

4.2 Spin-Boson Hamiltonian description

The physical interpretation of θ can obtained by utilizing Hamiltonian based alternative description of correlated decoherence. The noise process, governed by the joint-evolution of the system of qubits and the environment is expressed by the sum of three Hamiltonians $H = H_Q + H_E + H_{int}$. The H_{int} describes evolution of qubits-environment coupling, H_E represents independent evolution of environment whose details will be briefly discussed shortly, while H_Q realizes ideal quantum circuit which maps to syndrome measurement cycle in our study. Now if error propagation is treated separately from the physical noise model, CNOT gate evolution component, responsible for qubit-qubit interaction, can be safely dropped from H_Q. This is because ideal CNOT gate, between data and ancilla qubits, only accounts for the X-stabilizer measurement which acts trivially on the joint Hilbert space of the operand qubits. The resulting simplified H_Q has been extensively studied [23, 42, 41, 10] and allows us to (i) explicitly specify Hamiltonian with relevant physical parameters (ii) develop closed-form solution expressing decoherence due to qubits collective coupling to the environment (iii) find probability distribution of errors due to the correlated noise.

In the spin-boson model, a two-level spin-1/2 particle represents a qubit whose

initial state is an +1 eigenstate of operator σ_z. For single qubit case $H_Q = \frac{\epsilon}{2}\sigma_z$ where constant ϵ signifies Zeeman's energy. The environment is a quantized (magnetic) field consisting of $\mathbf{k}$ modes, each modeled as quantum harmonic oscillator associated with frequency $\omega_{\mathbf{k}}$. The evolution of environment follows $H_E = \sum_{\mathbf{k}} \omega_{\mathbf{k}} b_{\mathbf{k}}^\dagger b_{\mathbf{k}}$ where $b_{\mathbf{k}}$ and $b_{\mathbf{k}}^\dagger$ are creation and annihilation operation respectively. The qubit decoherence arises from its coupling with the field modes, the parameter $g_{\mathbf{k}}$ accounts for its coupling strength with mode $\mathbf{k}$, then $H_{int} = \sum_{\mathbf{k}} \sigma_z (g_k b_k^\dagger + g_k^* b_k)$. The complete Hamiltonian $H = H_Q + H_E + H_{int}$ will be written as:

$$H = \tfrac{\epsilon}{2}\sigma_z + \textstyle\sum_{\mathbf{k}} \omega_k b_k^\dagger b_k + \sum_{\mathbf{k}} \sigma_z (g_k b_k^\dagger + g_k^* b_k)$$

The environment temperature T describes the magnitude of its thermal fluctuations which exchange energy with the qubit. The coherence decay contributed by mode $\mathbf{k}$ for time t has a known closed-form expression: $\exp\{-|g_{\mathbf{k}}|^2 \frac{1-cos(\omega_{\mathbf{k}} t)}{1-\omega_{\mathbf{k}}^2} \coth(\frac{\omega_{\mathbf{k}}}{2T})\}$ [23]. In the limit of continuum $\omega_{\mathbf{k}}$, the subscript $\mathbf{k}$ is dropped and $g_{\mathbf{k}}$ is conveniently expressed as its spectral density function $G(\omega)$ of continuous variable ω of the form $G(\omega) = \omega^s e^{-\omega/\omega_c}$ [42], where positive valued s and the cut-off frequency ω_c are device specific constants. For ohmic environment ($s = 1$), the amplitude of single qubit coherence decays as $e^{-L(t)}$ [23], where time dependent parameter $L(t)$ in (1) is obtained by integrating the decoherence contribution from all field modes (i.e. $\omega \in [0, \infty]$) in thermal equilibrium state.

$$L_d(t) = A \int_0^\infty \omega e^{-\omega/\omega_c} \frac{1 - cos(\omega t)}{1 - \omega^2} \coth(\frac{\omega}{2T}) d\omega \tag{1}$$

The underlying physics of decoherence process is driven by the timescale t [42] which depends on device parameters (T, ω_c) in (1). The qubit exposed to the environment for short enough time: $t < \omega_c^{-1}$, suffers from negligible decoherence since environment rarely oscillates at high frequency. However when qubit-environment interaction spans over very longer time scale: $t > T^{-1}$, the intrinsic thermal oscillation allows environment to actively exchange spin energy with the qubit causing T_1 type decoherence [23] (e.g. amplitude damping noise). We assume no change in the population (diagonal elements of density matrix) thus T_1 decay irrelevant. Instead, the increasing gate speed [30] and rapidly improving qubit shielding techniques [24] shown in the recent quantum device technologies, naturally motivate us to restrict our model to realistically shorter timescale. Hence we choose the regime $\omega_c^{-1} < t < T^{-1}$ of T_2 type decoherence which diminishes the off-diagonal terms only.

The collective dephazing of the multi-qubits system containing n-qubits also depends upon spatial location d_l of l_{th} qubit. If $\sigma_{z,l}$ is the Z-stabilizer for the l^{th} qubit, the n-qubits collective dephazing Hamiltonian is reshaped after Ref[42] as follows:

$$H = \tfrac{\epsilon}{2} \textstyle\sum_{l=0}^{n-1} \sigma_{z,l} + \sum_{\mathbf{k}} \omega_k b_k^\dagger b_k + \sum_{\mathbf{k},l} \sigma_{z,l} (g_k e^{i\mathbf{k}.\mathbf{d}_l} b_k^\dagger + g_k^* e^{-i\mathbf{k}.\mathbf{d}_l} b_k)$$

The expression of closed-form solution involves qubits pairwise coupling to the environment. Let d_l and d_m are the corresponding positions of qubit l and m with respect to the environment, then using previously defined frequency domain snapshot of the coupling $g_{\mathbf{k}}$: $G(\omega) = \omega^s e^{-\omega/\omega_c}$, L_d in (1) will become also a function of qubits pairwise-distance $d_{l,m} = |d_l - d_m|$ [32]

$$L_d(t, d_{l,m}) = A \int_0^\infty \omega e^{-\omega/\omega_c} \frac{1-cos(\omega t)}{1-\omega^2} \coth(\frac{\omega}{2T}) \frac{\sin(\omega d_{l,m})}{\omega d_{l,m}} d\omega$$

Thus if $\rho(0) = \frac{1}{2^n} \sum_{x,y \in Z_2^n} |x\rangle\langle y|$ is the initial state of n-qubits system then after decohering for time t the final state $\rho(t)$ can be found in (2)

$$\rho(t) = \frac{1}{2^n} \sum_{x,y \in Z_2^n} e^{-C_{x,y}} |x\rangle\langle y| \tag{2}$$

$C_{x,y}$ captures the decay of $|x\rangle\langle y|$ coherence in time and space, and is expressed as $C_{x,y} = |\sum_{i,j}(x_i - y_j)|^2 L(t, d_{l,m})$. Thus θ in our model maps to $\sqrt{L(t, d_{l,m})}$ in spin-boson case [42, 32]. We can alternatively express $C_{x,y}$ in more simplification friendly form:

$$C_{x,y} = \sum_{l,m}(x_l - y_l)(x_m - y_m) L(t, d_{l,m})$$

Note that in case of independent noise, $C_{x,y}$ does not depend on d and reduces to $\sum_l |x_l - y_l| L(t)$ [42]. At this point we refer back to the gray-scale map of a 13-qubits surface code density matrix in Figure-1. The map whitens each coherence $|x\rangle\langle y|$ in proportion to its amplitude decay and reveals insightful comparison of fidelity loss governed by correlated noise with that by its independent counterpart. In former model, higher fluctuations in amplitude decay, indicated by distinguishable black and white sub-regions, sharply contrasts with nearly homogeneously gray trends of fidelity in the latter. This example clearly establishes that noise correlations lead to significantly larger variations in the amplitude of coherences.

4.3 Probability distribution over correlated errors in single operation

In order to find expression of probability distribution over correlated errors, we simplify the correlation parameter $L(t, d_{l,m})$ under reasonable assumptions. We set t in $C_{x,y}$ equal to the time taken by the single operation such as state preparation, CNOT or Measurement (assuming each takes single time-step for execution) in a single trial of surface code syndrome measurement shown in the dotted box of Figure-2. Therefore by assigning code specific constant to t, both $L(d_{l,m})$ and $C_{x,y}$ become

functions of qubits' pairwise separation. We further assume qubit-environment interaction falls in the *superdecoherence* regime [42] in which all the qubits in the logical block to couple with the environment with the approximately same strength. Since coupling strength is position sensitive, for superdecoherence regime to hold for increasing number of qubits, the separation $d_{l,m}$ between any qubits pair is essentially upper-bounded by constant distance d. This allows us to holistically adjust magnitude of noise spatial correlation by working with single parameter $L_d \equiv L(d)$. In Section-6, we analyze a worst-case scenario which tests quantum error correction with maximal spatial noise correlation occurring in the limit $d = 0$. To further simplify (2), we rewrite $C_{x,y} = \sum_{l=m}(x_l - y_l)(x_m - y_m)L_d + \sum_{l\neq m}(x_l - y_l)(x_m - y_m)L_d$. The first term in the summation becomes $|x \oplus y|L_0$ (here $|.|$ denotes the hamming weight), while second term reduces to $(|x| - |y|)^2(L_d - L_0)$. Therefore $C_{x,y}$ simplifies to the form in (3).

$$C_{x,y} = |x \oplus y|(L_0 - L_d) + (|x| - |y|)^2 L_d \tag{3}$$

We choose the n-qubits state in (2) containing superposition of codewords and non-codewords in order to evaluate Kalai's skepticism [26] of fault-tolerant quantum computation; that the presence of non-codewords should fail the error correction. However, we assume that when the logical qubit is projected into the code basis states during error correction, the non-codewords translate into bit-flip errors. This enables us to analyze the performance of dephasing noise averaged over all patterns of bit-flip errors. The dephasing noise also discretizes into a specific set of k-qubits in phase-flip (Z) errors, with probability $\Pr_k$ obtained from projective quantum measurement expression: $\Pr_k = \mathrm{Tr}(X_k X_k^\dagger \rho(t))$. Here $X_k := \frac{1}{2^n}\sum_{x,y\in Z_2^n}(-1)^{k.(x\oplus y)}|x\rangle\langle y|$ represents X-syndrome measurement operator (explained in Section-5) which identifies a set of k-qubits in Z-errors. Note that the operator X_k also represents density matrix of the pure superposition state of the n-qubits containing known k-phase flip errors. In this sense, the projection can also be interpreted as the square of fidelity between $\rho(t)$ and X_k. Next, since all possible syndrome measurement outcomes are mutually exclusive and exhaustive, by completeness $\sum_k X_k X_k^\dagger = I$. It is straightforward to verify that X_k is symmetric by definition: $X_k^\dagger = \frac{1}{2^n}\sum_{y,x\in Z_2^n}(-1)^{k.(y\oplus x)}|y\rangle\langle x|$ which is same as X_k by swapping x with y. More importantly X_k is also idempotent shown as follows:

$$\begin{aligned} X_k X_k &= \tfrac{1}{4^n}\textstyle\sum_{x,y\in Z_2^n}(-1)^{k.(x\oplus y)}|x\rangle\langle y|\sum_{x',y'\in Z_2^n}(-1)^{k.(x'\oplus y')}|x'\rangle\langle y'|. \\ &= \tfrac{1}{4^n}\sum_{x,y,x',y'\in Z_2^n}(-1)^{k.(x\oplus y\oplus x'\oplus y')}|x\rangle\langle y|x'\rangle\langle y'| \\ &= \tfrac{1}{4^n}\sum_{x,x',y'\in Z_2^n}(-1)^{k.(x\oplus y')}|x\rangle\langle y'| = \tfrac{1}{2^n}\sum_{x,y'\in Z_2^n}(-1)^{k.(x\oplus y')}|x\rangle\langle y'| \end{aligned}$$

By renaming y' to y, we obtain $X_k X_k = X_k X_k^\dagger = X_k$ as claimed above. Next, we find $\mathrm{Tr}(X_k X_k^\dagger \rho(t))$ where $X_k X_k^\dagger \rho(t)$ resolves to

$$X_k X_k^\dagger \rho(t) = \tfrac{1}{4^n} \sum_{x',x,y \in Z_2^n} (-1)^{k.(x' \oplus x)} e^{-C_{x,y}} |x'\rangle\langle y|$$

The trace of the resulting matrix becomes

$$\mathrm{Tr}(X_k X_k^\dagger \rho(t)) = \tfrac{1}{4^n} \sum_{x',x,y \in Z_2^n} (-1)^{k.(x' \oplus x)} e^{-C_{x,y}} \langle x'|x'\rangle\langle y|x'\rangle$$

After simplification, we finally obtain $Pr_k = \mathrm{Tr}(X_k X_k^\dagger \rho(t))$

$$\mathrm{Pr}_k = \frac{1}{4^n} \sum_{x,y \in Z_2^n} (-1)^{k.(x \oplus y)} e^{-C_{x,y}} \tag{4}$$

The calculation of Pr_k using summation over Z_2^n in (4) incurs computational intractability due to exponential increase in n, the size of Hilbert space. Alternatively, the summation can be decomposed into the n-product terms over GF(2) for each of n-qubits in equal superposition of $|0\rangle$ and $|1\rangle$ state. Similarly, if the terms $(-1)^{k.(x \oplus y)}$ and $e^{-C_{x,y}}$ can be decomposed into bitwise products, the overall computational workload involving only n-tensor products can be handled efficiently. While the factorization of $(-1)^{k.(x \oplus y)}$ into bitwise products can be easily attained: $\prod_{l=1}^{n} (-1)^{k_l.(x_l \oplus y_l)}$, the product resolution of $e^{-C_{x,y}}$ entails algebraic simplification of $e^{-(|x|-|y|)^2 L_d}$. We note that $e^{-(|x|-|y|)^2 L_d}$ is a moment generating function obtained from solving $E[e^{-2i(|x|-|y|)z}]$ where $Z \sim \mathcal{N}(0, \frac{L_d}{2})$. Expanding the function integral yields $\frac{1}{\sqrt{\pi L_d}} \int_{-\infty}^{\infty} e^{-\frac{z^2}{L_d}} e^{-2iz(|x|-|y|)} dz$. Thus (4) becomes:

$$\mathrm{Pr}_k = \tfrac{1}{4^n} \int_{-\infty}^{\infty} e^{-\frac{z^2}{L_d}} \sum_{x,y \in Z_2^n} (-1)^{k.(x \oplus y)} e^{-|x \oplus y|(L_d - L_0) + 2iz|x| - 2iz|y|} dz$$

Substituting bitwise n-fold product over Z_2 for the summation over Z_2^n gives

$$\mathrm{Pr}_k = \tfrac{1}{4^n} \int_{-\infty}^{\infty} e^{-\frac{z^2}{L_d}} \prod_{l=1}^{n} \sum_{x_l,y_l \in Z_2} (-1)^{k_l.(x_l \oplus y_l)} e^{-|x_l \oplus y_l|(L_d - L_0) + 2iz|x_l| - 2iz|y_l|} dz$$

If we define $q(k_l) = \sum_{x_l,y_l \in Z_2} (-1)^{k_l.(x_l \oplus y_l)} e^{-|x_l \oplus y_l|(L_d - L_0) + 2iz|x_l| - 2iz|y_l|}$, then

$$q(0) = \sum_{x_l,y_l \in Z_2} e^{-|x_l \oplus y_l|(L_d - L_0) + 2iz|x_l| - 2iz|y_l|} = 2(1 + e^{-(L_0 - L_d)} \cos(2z))$$

Similarly $q(1) = 2(1 - e^{-(L_0 - L_d)} \cos(2z))$. By letting $\tilde{p}_z = \frac{1}{2}(1 - e^{-(L_0 - L_d)} \cos(2z))$ then $\frac{1}{4} q(1) = \tilde{p}_z$ while $\frac{1}{4} q(0) = 1 - \tilde{p}_z$. Since there are $|k|$ product terms of $\tilde{p}_z$ for

each of the k-qubits in error and the remaining $(1-\tilde{p}_z)$ product terms for each of the $n-|k|$ error free qubits, the probability $\Pr_k$ simplifies to (5)

$$\Pr_k = \frac{1}{\sqrt{\pi L_d}} \int_{-\infty}^{\infty} e^{-\frac{z^2}{L_d}} \, \tilde{p}_z^{|k|} (1-\tilde{p}_z)^{n-|k|} dz \tag{5}$$

The integral of (5) conveniently expresses probability of spatially correlated errors using the expectation of independent probability of errors acting as a function of a normal random variable z. Since the complexity of solving the integral scales only linearly with the number of qubits i.e. n, the expression (5) is crucial to scale our statistical analysis to higher distance surface code. The Figure-6 plots $\Pr_k$ against $|k|$: the number of qubits in error for different values of correlation parameter L_d for distance nine ($cd = 9$) surface code. The curve for $L_d = 0$ (independent noise) gradually departs from uniformly exponential decline and shows the flatter tail with increasing L_d. The flat ended correlated noise curve assigns significantly higher probability to the occurrence of many-qubits errors. This is evident from the exponentially increasing gap between the probability of *any* $|k|$-qubits errors for both the correlated (for $L_d = L_0$) and the independent noise curves in Figure-7. The widening gap indicates that the probability of $|k|$-qubits errors decreases sub-exponentially (in $|k|$) in spatially correlated noise.

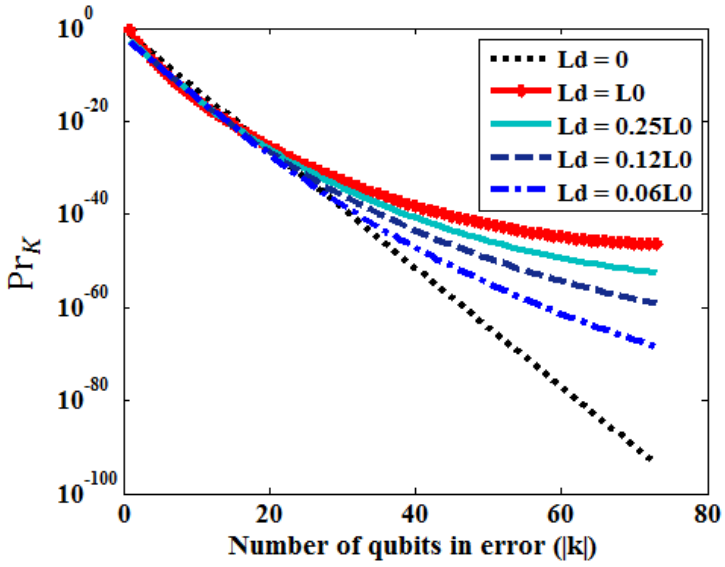

Figure 6: (Color online) The probability of given $|k|$-qubits errors: $\Pr_k$ plotted against $|k|$ for various strengths of correlated noise parametrized by L_d. The correlation strength increases from $L_d = 0$ for independent noise to $L_d = L_0$ for maximal noise correlation

It should be noted that $\Pr_k$ is invariant under unitary operation U on the qubits. Therefore both the density matrix $\rho(t)$ and projection operators X_k, $X_k^\dagger$ and transformed into $U\rho(t)U^\dagger$, $UX_kU^\dagger$ and $U^\dagger X_k^\dagger U$ respectively. The entire product $X_kX_k^\dagger\rho(t)$ is transformed as:

$$UX_kX_k^\dagger\rho(t)U^\dagger = \tfrac{1}{4^n}\sum_{x',x,y\in Z_2^n}(-1)^{k.(x'\oplus x)}e^{-C_{x,y}}U|x'\rangle\langle y|U^\dagger$$

whose trace is

$$\begin{aligned}\mathrm{Tr}(UX_kX_k^\dagger\rho(t)U^\dagger) &= \tfrac{1}{4^n}\sum_{x',x,y\in Z_2^n}(-1)^{k.(x'\oplus x)}e^{-C_{x,y}}\langle x'|U^\dagger U|x'\rangle\langle y|U^\dagger U|x'\rangle \\ &= \tfrac{1}{4^n}\sum_{x',x,y\in Z_2^n}(-1)^{k.(x'\oplus x)}e^{-C_{x,y}}\langle x'|x'\rangle\langle y|x'\rangle \\ &= Tr(X_kX_k^\dagger\rho(t))\end{aligned}$$

which gives $\Pr_k$ same as in (4). During syndrome measurement cycle the only unitary operation U is the CNOT gate between data and the ancilla qubits. Therefore its exclusion from the physical noise model leaves probability distribution over errors unchanged. Finally, note that the ideal non-unitary operations, such as state-preparation and Measurement, do not map to Hamiltonian evolution and thus can be safely ignored in the physical noise model.

4.4 Per-operation qubit error probability

Next we show that the two physical quantities L_d and L_0 can be subsumed under single quantity called *per- operation qubit error probability* adequately captures the noise strength in both the models. We first define this scale for independent noise and then extend it applicability to the correlated model. In the former model, the correlation parameter L_d remains naught throughout i.e. $L_d = 0$, whereas in latter $L_d > 0$, while $L_0 > 0$ always. The disappearance of L_d in the independent noise case, can be interpreted both physically and mathematically. The physical interpretation of this limiting case $L_d = 0$ can be explained by (3). There are two components of noise appearing as exponent $C_{x,y}$; one component that accounts for the individual qubit interaction with the distinct environment represented by the co-efficient of L_0 and the other one is the qubits pair-wise (correlated) interaction with the same environment contained in the co-efficient of L_d. Naturally as $L_d = 0$, the correlated component disappears, leaving us with decoherence due to independent noise only: $C_{x,y} = |x \oplus y|L_0$.

Mathematically when $L_d = 0$, the probability density function $z \sim \mathcal{N}(0, \frac{L_d}{2})$ shrinks entirely to its mean value i.e. $z = 0$. Then $\Pr_{|k|} = \tilde{p}_z^{|k|}(1-\tilde{p}_z)^{n-|k|}|_{z=0}$ where $\tilde{p}_z|_{z=0} = \frac{1}{2}(1-e^{-L_0})$ defines the probability that k out of n qubits independently

fail. Notice that $\tilde{p}_z$ which was originally a function of random variable $z \sim \mathcal{N}(0, \frac{L_d}{2})$ in (5), is now reduced to a deterministic function of L_0. Thus when $L_d = 0$, $\tilde{p}_z$ can account for the magnitude of independent noise. When $L_d > 0$ in case of correlated noise, $\tilde{p}_z$ assumes its general form of a random variable which warrants its statistical characterization. The expected value of $\tilde{p}_z$ calculated w.r.t z, describes mean amplitude decay (4) of coherences in $\rho(t)$ subject to the correlated noise. Let $p_z \equiv E_z[\tilde{p}_z]$, then by substituting $\tilde{p}_z = \frac{1}{2}(1 - \cos(2z))$ for maximal noise correlation (i.e. when $L_d = L_0 > 0$), we obtain basic expression of p_z as follows:

$$p_z \approx \frac{1}{2\sqrt{\pi L_0}} \int_{-\infty}^{\infty} (1 - \cos(2z))\ e^{-\frac{z^2}{L_0}}\ dz|_{L_0 = L_d}$$

In sub-threshold region the expected noise strength L_0 is a small value, usually less than 0.05 [20]. Hence the bulk of area under $z \sim \mathcal{N}(0, \frac{L_0}{2})$ curve is concentrated near $z \approx 0$. In this limit, the low order Taylor Series approximation $cos(2z) \approx 1 - 2z^2$ simplifies the integral and reduces it to the variance of z. In algebraic terms:

$$p_z \approx \frac{1}{\sqrt{\pi L_0}} \int_{-\infty}^{\infty} z^2\ e^{-\frac{z^2}{L_0}}\ dz = \frac{L_0}{2}|_{L_0 = L_d}$$

After recognizing that $\frac{1}{2}(1 - e^{-L_0}) \approx \frac{L_0}{2}$ when L_0 is small, we write the final expression of p_z in (6)

$$p_z \approx \frac{1}{2}(1 - e^{-L_0})|_{L_0 = L_d} \tag{6}$$

Conclusively, we have found single scale which can weigh noise magnitude in both models and facilitates fair quantum error correction performance comparison. The scale p_z can be interpreted as *per-operation probability of the phase-flip error in the qubit*, independent of the other qubits in the quantum computer. The identification of a suitable scale plays pivotal role in the faithful evaluation of quantum error correction under noise correlation. Following subsection summarizes crucial merits of p_z.

4.4.1 Crucial merits of per-operation qubit error probability: p_z

1. It quantifies the strength of noise in both the independent and correlated noise models in the sub-threshold region where noise level remains low. In this region, any change in the noise strength due to either independent ($L_d = 0$) or correlated ($L_d = L_0 > 0$) interaction with the environment, will faithfully reflects proportional change in p_z. Hence, instead of tweaking two variable separately, changing single variable p_z to vary noise strength suffices. This scale defines the horizontal axis of the threshold region logical failure probability plots and substantially simplifies our fault-tolerance analysis.

2. By quantifying L_d, it obviates cumbersome task of directly measuring noise correlation in the physical quantum device. When L_d translates into p_z in (6), correlation magnitude can be feasibly obtained from the experimental knowledge of the failure rate of the qubit.

3. It also maps to one of the most generic and widely used metric of decoherence: the (in)fidelity. By definition, the fidelity F between the noisy state ρ and pure(noiseless) state $|\phi\rangle$ is given by $F = \sqrt{\langle\phi|\rho|\phi\rangle}$. In our case $F = \sqrt{\frac{1}{4^n}\sum_{x,y\in Z_2^n} e^{-C_{x,y}}}$ or $F = \sqrt{\Pr_0}$. The $\Pr_0$ depends only on L_d and L_0, which in turn can be derived from p_z using (6).

4. By virtue of its mapping on fidelity, it can be applied to variety of quantum computing devices. Since fidelity can be measured from wide range of known tomography techniques [58, 39], one can obtain p_z using off-the-shelf experimental methods already designed for several quantum device technologies. Therefore p_z can be deployed to evaluate fault-tolerance properties across several candidates of fault-tolerant quantum hardwares subject to correlated noise, without explicitly measuring the subtle correlation strength!

4.5 Probability distribution over correlated errors in multiple operations

We conclude this section by expanding our model to incorporate temporal noise correlation among multiple operations on the qubits during error correction. As it stands, $\Pr_k$ defined in (5) describes the probability of k out of n qubits-errors during single operation. In order for Pr_k to include the probability distribution of time-correlated errors, it will be helpful to first understand the nature of time-correlated noise using Figure-4. Each time an operation is performed, the operand qubit i is exposed to the environment E; the errors due to faulty gate operations are attributed solely to the qubit-environment interaction. A noisy gate translates into noiseless gate (not shown) immediately followed by $CR_{i,E}$ gate shown in Figure-4.

Next, we define the length of temporal correlation called *environment memory span* as the number of qubit operations time-steps for which qubit-environment joint wave-function continues to evolve unitarily before its eventual collapse by the Measurement. The Figure-4 depicts N qubit-operations long environment memory span leads to the same number of qubit-environment interactions. The coherence of qubit i naturally decays as a function of n. It is straightforward to show that if the qubit is assumed to be shielded from the bit-flip, it constructively accumulates the N-phase displacements (i.e. $N\theta$) till the Measurement. Under this assumption, we find that the amplitude of the non-diagonal term of the qubit density matrix decays $\cos(N\theta)$ ($\approx \exp(-\frac{1}{2}N^2\theta^2)$ when $N\theta$ is small). By substituting $N\theta$ for θ and repeating the entire algebra from (3) to (5), we derive the probability that k out of n qubits in error during N sequential operations denoted by $\Pr_k^{(N)}$ in (7).

$$\Pr_k^{(N)} = \frac{1}{\sqrt{\pi L_d^{(N)}}} \int_{-\infty}^{\infty} e^{-\frac{z^2}{L_d^{(N)}}} \tilde{p}_{z(N)}^{|k|} (1 - \tilde{p}_{z(N)})^{n-|k|} dz \tag{7}$$

In (7), $L_d^{(N)} = N^2 L_d$, $\tilde{p}_{z(N)} = \frac{1}{2}(1 - e^{-N^2(L_0 - L_d)} cos(2z))$. Along these lines, we can define quantity: *per N-operations qubit error probability* $p_{z(N)}$ which is obtained by substituting $N^2 L_0$ for L_0 in (6) for the case of multiple operations. Therefore, $p_{z(N)}$ can be interpreted as p_z accumulated over N sequential operations on qubit i of Figure-4. This accumulation which is linear (NL_0) in independent noise, becomes quadratic($N^2 L_0$) due to time-correlated errors. Consequently, the probability of individual qubit error rises quadratically in the number of sequential operations suffering from temporal noise correlation.

The convoluted spatial-temporal noise $\Pr_k^{(N)}$ in (7) describes probability of $k \leq n$ qubits in errors by the end of N-operations. However, it should be cautioned that $\Pr_k^{(N)}$ only describes probability distribution of errors, not the spatial or temporal identity of errors. Once dissolved into single parameter $L_d^{(N)}$, the time and space connotation of noise becomes less distinguishable; a given qubit error may have occurred due to spatial, temporal or joint spatial-temporal noise correlation. Therefore, one cannot easily decompose set of k-errors into non-overlapping sets space and time-correlated errors. The choice of our environment memory span is dictated by the structure of the quantum error correction; it is set equal to three operation time-steps i.e. $N = 3$ to execute single trial of syndrome extraction terminating in the measurement of $|Ancilla\rangle$ as shown in Figure-2. Note that the environment memory span allows single operation on $|Data\rangle$ and three operations on $|Ancilla\rangle$ respectively.

By extending environment induced time dependent decoherence to our initially spatially correlated noise, the final version of the model (7) can be categorized *long-range non-Markovian* in the context of prior work on correlated noise (summarized in Section-2). Long-range behavior can be attributed to the coupling of *all*, including distant codeword qubits, to the same environment during each operation time-step. It is non-Markovian because it allows errors to correlate across multiple operations time-steps during syndrome extraction trial. Such error-correction-centric correlated model has not received adequate attention in the prior studies and features novel contribution of this work.

It is reminded that for the comparative performance analysis, we employ same definition of independent noise as that in the prior studies on surface code fault-tolerance. We define independent noise model as a type of noise which permits *no* spatial or temporal noise correlations among errors or fault-paths. This model can be realized by allocating unique environment for each codeword qubit. The environments of different qubits are forbidden to interact with each other and are periodically refreshed after each operation time-step. Consequently, the environment exhibits only short-term memory and ascribes Markovian behavior to the noise. The fault-tolerance proofs of surface code [9, 18, 51, 53, 14] are all based on this definition of

independent noise.

To highlight its sharp contrast with independent noise, we summarize salient attributes of our correlated noise model below:

1. A noisy quantum operation couples operand qubit(s) to the same non-Markovian environment.

2. The qubit-environment interaction results in the phase-flip errors on the qubits. Our analysis of fault-tolerance concerns the detection and correction of only phase-flip error.

3. The CNOT gates in the syndrome measurements propagate phase-flips only from data to ancilla which is tracked in line-5 of our decoding algorithm (Algorithm-1). There is no propagation of errors from ancilla to data.

4. The execution of noisy operation U on qubit i is modeled as the application of noiseless operation U_{ideal} followed by qubit-environment interaction $CR_{i,E}$ (Figure-4). Therefore $U = CR_{i,E}U_{ideal}$ The errors resulting from this interaction $CR_{i,E}$ are separately handled, propagated and tracked in the decoding algorithm (Algorithm-1). Then U_{ideal} will act trivially on the (joint Hilbert space of data and ancilla) qubits state without altering the probability distribution of errors.

5. A faulty Measurement of qubit i is modeled as the application of $CR_{i,E}$ followed by the ideal Measurement.

6. Environment memory span lasts for three operations during single trial of syndrome measurement which culminates in the Measurement of ancilla. Since environment and ancilla qubits are synchronously Measured and refreshed, a specific set of correlated errors on ancilla qubits (or on data-ancilla qubits) is unlikely to survive [57, 41] multiple trials of syndrome measurements. Such low probability correlated errors are ignored due to the ephemeral role of the ancilla in error-correction and concomitantly short-lived environment assumed in the noise model.

7. During syndrome measurement cycle, qubits acquire spatial and temporal errors whose probability mass function is given by (7).

5 Brief Overview of Surface Code Error-Correction

Surface code is hailed one of the most celebrated breed of topological quantum error correcting codes [9] and is known for high threshold [45, 19, 51] as well as hardware implementation-friendly geometry [18]. A block of logical qubit connects information bearing qubits (called data qubits) in a 2-D nearest-neighbor architecture compatible

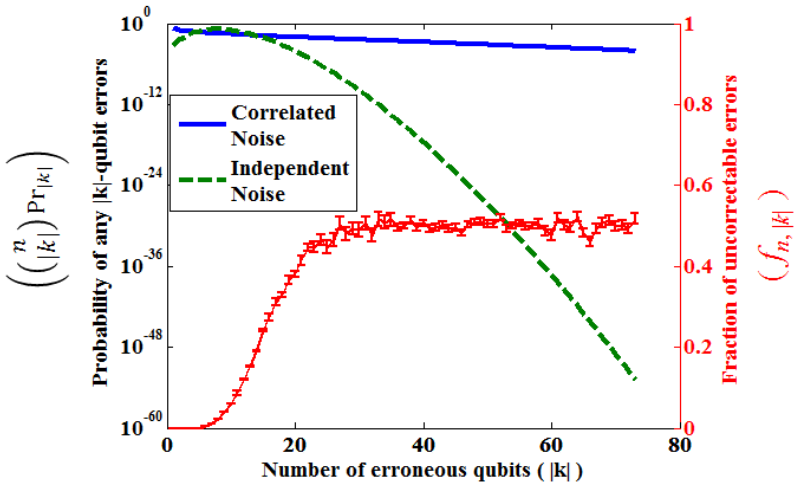

Figure 7: (Color online) [Left vertical axis] Probability mass function of $|k|$-qubits errors for maximally correlated ($L_d = L_0$) and independent ($L_d = 0$) noise cases selected from Figure-6. [Right vertical axis] The fraction $f_{n,|k|}$ of uncorrectable $|k|$-qubits errors. The error-bars quantify variance in the data

with the device-level connectivity constraints of several quantum hardware technologies. Once logical qubit is prepared in desired state, a chronological three-step error correction proceeds as follows (1) Error-detection measures parity-check operators on data qubits located in the neighborhood of ancillary qubit which stores syndrome. (2) Error-decoding maps the obtained set of syndromes to the most likely set of erroneous data qubits. (3) Recovery of logical qubit state applies appropriate Pauli gates to cancel the errors in qubits. In case of incorrect decoding, the application of the gates produces a chain of undetectable errors connecting opposite boundaries of the code block, resulting in the logical error. The performance of the surface code is mainly dictated by the length of uncorrectable chain of data-qubits errors. Higher performance can be achieved when longer chain of errors are needed to connect the opposite boundaries. This is accomplished by increasing the distance (the number of qubits) between the opposite boundaries of the code block by adding more qubits along both horizontal and vertical axes. This characteristic distance, labeled with cd, is the known as the code-distance of the surface error correcting code. The increased code-distance stipulates longer, therefore, less probable chains of errors causing logical failures. For example, if an error independently hits each data-qubit error with small probability p, the occurrence of logical failure to the lowest order in p becomes $O(p^d)$ [18] where $d = \frac{cd+1}{2}$ for odd values of cd. Hence the fault-tolerance in surface code can be achieved by exponentially lowering the logical failure probability by nominally incrementing the code distance [19, 51, 53, 14].

The precise quantification of the logical failure probability entails exhaustive counting of all possible combinations of errors which directly or indirectly produce logical error. Such brute force counting becomes computationally intractable due to exponentially increasing combinations for the larger code-distance surface codes. Alternatively, a more practical approach can be applied; by sampling from the set of the *most* relevant combinations of errors. These are usually short in size (e.g. errors combinations of size around $\frac{cd+1}{2}$) and comprise significant component of the logical failure probability. The resulting low order approximation of the logical failure probability suffices for the analysis of the sub-threshold ($p \leq p_{th}$) region of the independent noise model [19].

We modify this approach in the light of correlated noise; by caring for sampling from longer combinations of errors. Our scheme samples errors set from the distribution that matches correlated noise curve in Figure-7 so that many-qubit errors combination properly enter the logical failure probability computation. Each randomly selected combination (now called set) B of error is tested for the logical error according to Algorithm-1. The set B is hidden from the decoding procedure and acts as a yardstick for the correct identification of errors. Then without any knowledge of B, the syndromes information is decoded into the most likely set of errors M using minimum weight perfect matching algorithm similar to Ref [19] shown in line 8 (of Algorithm-1). The two sets are compared and merged together to construct new set $B = (B \setminus B \cap M) \cup (M \setminus M \cap B)$ (line 17). The success or failure of error-correction depend upon the composition of set B for three cases: (i) $B = \{\}$ indicates correct decoding of errors, thus no logical failure (ii) B contains chain of errors which commutes with all X-Stabilizers but does not belong to the linear combinations of Z-Stabilizer (line 23). This results in the logical error as shown Figure-8. (iii) B is neither empty nor contains logical error but maps to the benign chain of errors as shown in Figure-9. The existence of such chain is confirmed by matching errors to the linear combination of Z-stabilizers and it involves solving a system of linear equations of the form $Az = b$ over GF(2) (line 19). Here A is the $2n + 1 \times n$ binary matrix whose non-zero elements of column i correspond to the qubits indices of i^{th} Z-Stabilizer. The $2n+1$-bits long column vector b encodes indices of erroneous qubits at its non-zero entries, while n-bits solution vector z will reveal the linear combination of Z-Stabilizers that constructs the error set B. If solution exists, then B comprises benign chain of errors which is not counted towards logical error event. Otherwise, the entire procedure reiterates by finding syndromes for the updated set B (line 5) until any one of the aforementioned three terminating conditions is satisfied (line 4).

Apart from the data-qubits errors, faulty syndrome extraction can also lead to logical error. The syndromes are stored and processed by the ancilla-qubits denoted by X in Figure-8. The syndrome extraction steps, depicted in Figure-8, subject data-qubits to Stabilizer measurement and culminate in syndrome registering its vote (error or no-error) in the final state ($|0\rangle$ or $|1\rangle$) of corresponding ancillary qubit X. A single trial of syndrome measurement may probabilistically fail due to errors

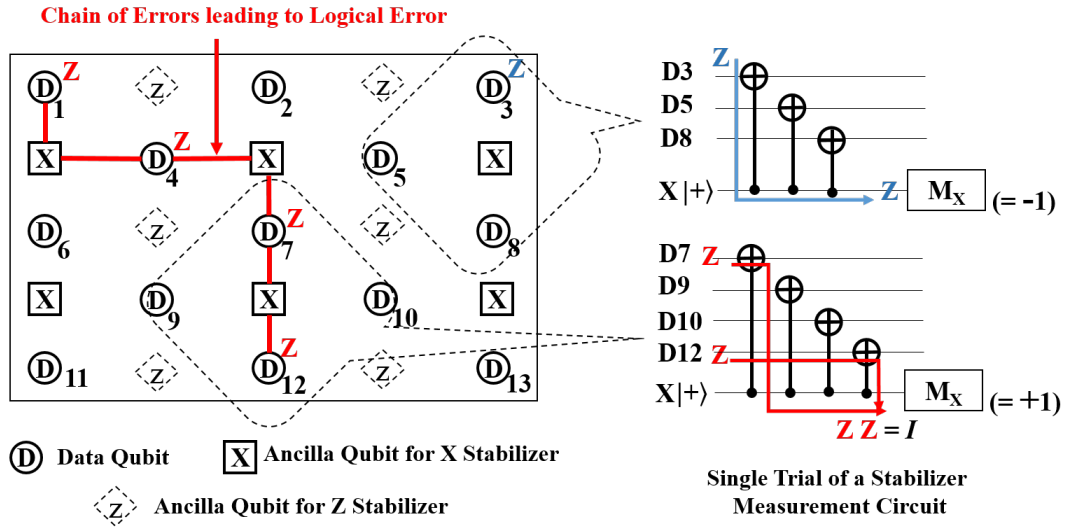

Figure 8: (Color online) Surface code architecture and error-detection procedure. An error on data qubit D3 can be correctly detected while the chain of errors on D1, D4, D7 and D12 result in undetectable logical error

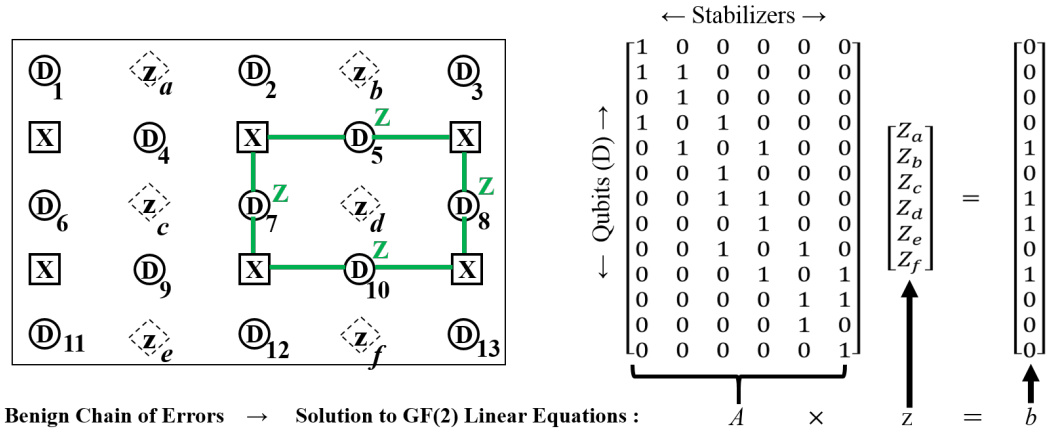

Figure 9: (Color online) The method of confirming the existence of benign errors by solving binary linear equations

in the qubit X during $|+\rangle$ state preparation, CNOT gates or Measurement. The reliability of syndrome is increased by thrice repeating Stabilizer measurement trial and obtain majority vote registered by each *copy* of X. These repetitions reduce the logical failure probability from ancilla errors, to $O(p^2)$ (when per-operation ancilla-qubit error probability is also p). To lower this logical failure probability sufficiently below $O(p^{\frac{cd+1}{2}})$, the entire syndrome extraction procedure (which includes three trials of Stabilizer measurement) is repeated $\frac{cd+1}{2}$ times. This prevents ancilla errors from becoming the performance bottleneck of the error correction.

In contrast to the case of data qubits, the logical failure probability due to ancilla errors can be calculated all analytically. During each trial of syndrome measurement, the temporal noise correlation spans three operations on the ancillary qubit, therefore the failure probability of each such trial can be calculated by letting $n = 1$, $N = 3$ and $k = 0$ in (7) to obtain $\Pr_0^{(3)}$. Then the probability p_T of the successful execution of trial involving single ancillary qubit is: $p_T = 1 - \Pr_0^{(3)}$. The correlation parameter $L_d^{(3)}$ is found by substituting p_z for p and $L_d^{(3)} (= L_0^{(3)})$ for L_0 in (6) and solving for $L_d^{(3)}$. Since three such trials comprise single round of syndrome measurement, their majority vote registers incorrect syndrome when two or more trials fail, the entire round then fails with probability $p_{\bar{S}} = 3p_T^2 + p_T^3$. Each round of syndrome extraction is executed cd times (Figure-2) and the logical failure is declared if it fails majority of times, which occurs with probability $p_{\bar{R}} = \sum_{i=(cd+1)/2}^{cd} p_{\bar{S}}$. By taking into consideration the spatial correlations among syndromes carrying n-ancilla qubits, we first solve (6) for L_0 when $p_z = p_{\bar{R}}$. Then using $L_d = L_0$, the logical failure probability of entire syndrome extraction process involving n-ancilla qubits is computed by (5) as $1 - \Pr_0$.

The next section compares the logical failure probability trends in the sub-threshold region of the two noise models for both data and ancilla qubits errors and highlights the most important contribution of this study.

6 Simulation Results

As discussed earlier, the logical failure probability P_L due to data-qubits errors, is estimated statistically and each statistic which determines the occurrence of logical failure using Algorithm-1, involves four-steps procedure (i) obtaining probability $\Pr_k$ of occurrence of specific set k of errors from (5) (ii) applying stabilizer measurements to map k to the syndrome set S_k (iii) executing minimum-weight perfect matching algorithm to decode most likely errors from S_k (iv) comparing decoded errors with actual error set (i.e. k) and establishing the outcome (logical success or failure) of the error correction. The P_L is then computed by multiplying $\Pr_k$ with the statistically calculated parameter $f_{n,|k|} \in [0, 1]$: the fraction of all possible combinations of $|k|$ errors ensuing the logical error. Hence for a code distance cd, the (8) expresses P_L as weighted sum of $\Pr_k$.

Algorithm 1: Our Surface Code Error Decoding Algorithm

Input: (i) A $2n+1 \times 2n+1$ surface code grid R which maps data-qubits to the grid vertices. The $2n+1$ data(qubits) vertices and n ancilla vertices for phase-flip syndromes are contained in sets D and S respectively (ii) Surface code $(2n+1 \times n)$ Z-Stabilizer binary matrix A (as shown in Figure-9) (iii) Surface code X-Stabilizer operators set $\{\mathcal{X}_i\}_{i=1}^{n}$ (iv) The set B of data-qubits errors

Output: $LogicalError \in \{True, False\}$

initialization $BenignError \longleftarrow False$, $LogicalError \longleftarrow False$, $S' \longleftarrow \{\}$

while $\neg$ *Benign Error* $\&\neg$ *Logical Error* $\& B \neq \{\}$ **do**

  $S' \longleftarrow$ Syndromes of B obtained by propagating errors from data to ancilla qubits

  $\forall\ i, j \in S'\ d_{i,j}^{min} \longleftarrow$ All pairs shortest path (S')

  Construct a complete graph $G(S', E)$ such that $\forall\ i, j \in S' \wedge e_{ij} \in E$, $|e_{ij}| = d_{i,j}^{min}$

  $S_{match} = \{(i,j) | i, j \rightarrow$ matched vertices in $S'\} \longleftarrow$ Minimum-weight matching(G)

  $M \longleftarrow \{\}$

  while $S_{match} \neq \{\}$ **do**

    $(i, j) \leftarrow$ next pair in S_{match}

    Find shortest path p_{ij} on grid R that connects i and j

    $M' \leftarrow \forall$ data vertices $q' \in p_{ij}$

    $M \longleftarrow M \cup M'$

    $S_{match} = S_{match} \backslash (i, j)$

  end

  $B \longleftarrow (B \setminus B \cap M) \cup (M \setminus M \cap B)$

  Define $b \in \{0\}^{2n+1}$ indexed by data vertices $\forall q' \in B$, $b[q'] = 1$

  if $\exists z \mid Az = b$ **then**

    $BenignError \longleftarrow True$

    else

      $\mathcal{B} \leftarrow Operator(b)$

      if $[\mathcal{B}, \mathcal{X}_i] = 0\ \forall i \in \{1, 2, .., n\}$ **then**

        $LogicalError \longleftarrow True$

      end

    end

  end

end

$$P_L = \sum_{|k| \geq cd} f_{n,|k|} \binom{n}{|k|} \mathrm{Pr}_k \tag{8}$$

For $p_z = 0.05$ and $cd = 9$ an example $f_{n,|k|}$ is plotted against $|k|$ on the right vertical axis of the graph in Figure-7. The curve which gradually rises from zero and eventually saturates to 0.5 for $|k| \geq 25$, clearly indicates that approximately half of many-qubits errors become logical errors. The small error bars show statistical variance in the data point of $f_{n,|k|}$ and hint at accumulation of statistical error while estimating P_L from (8). Since $f_{n,|k|}$ is the only statistically calculated component of each product term, the accumulated error is naturally dictated by the number of statistics and the confidence interval chosen for $f_{n,|k|}$. The accurate quantification of P_L requires that statistical error due to $f_{n,|k|}$ in each term of (8) is confined to acceptable limits. For a well-founded estimate, we choose 99% confidence interval whose width is at least two-orders of magnitude smaller than the value $f_{n,|k|}$. In our simulations, we noted that only the terms in the range: $\frac{cd}{2} \leq |k| \leq cd$ meaningfully contribute to P_L. Thus an overly circumspect choice of first hundred terms in (8), defines for P_L, a 95% confidence interval whose length is only $2 * 1.96 * \sqrt{100(\frac{0.01}{2*2.96})^2} = 0.066$ (6.6%) of the P_L value. Hence, we can say with 95% confidence that the error in our estimated P_L is 6.6%.

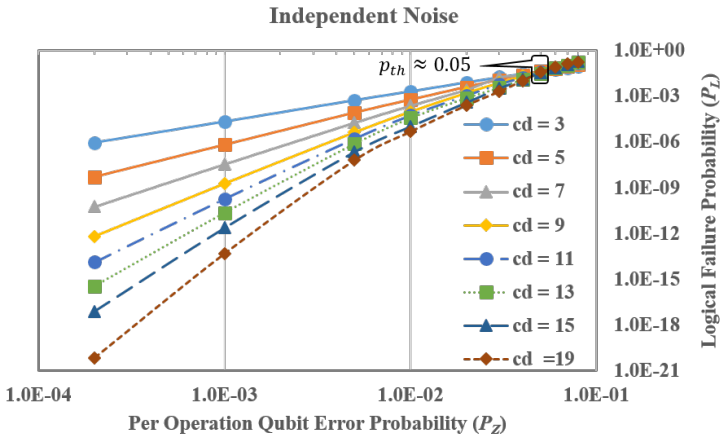

Figure 10: (Color online) The logical failure probability due to independent data-qubits errors, plotted against per-operation qubit error probability for increasing code-distances cd

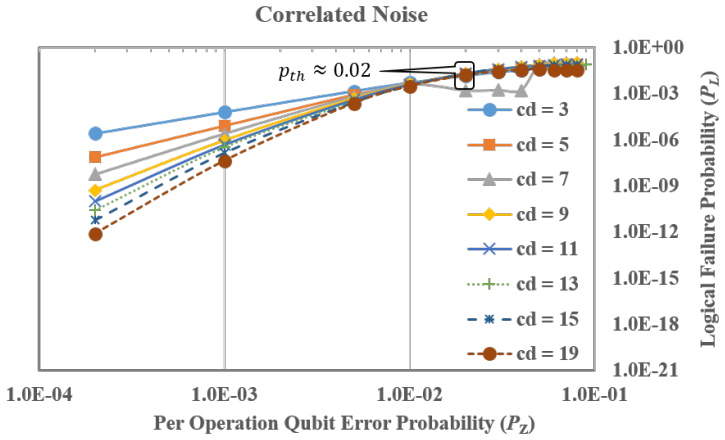

Figure 11: (Color online) The logical failure probability due to correlated data-qubits errors, plotted against per-operation qubit error probability for increasing code-distances *cd*

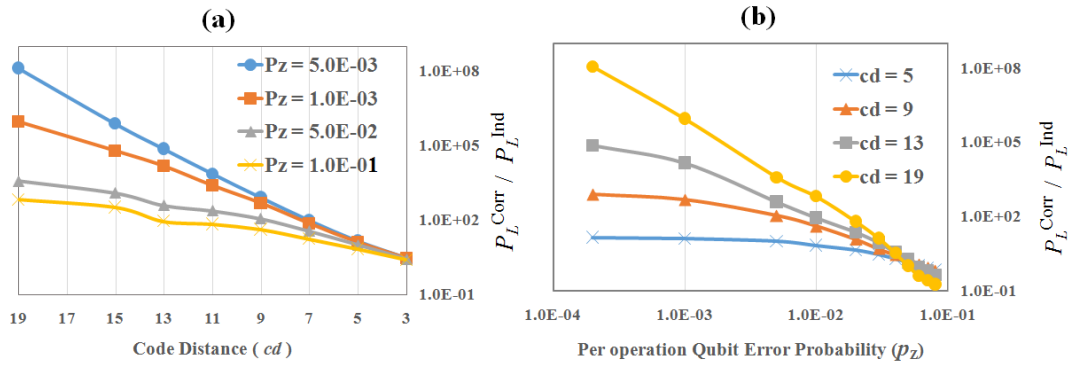

Figure 12: (Color online) The ratio between correlated and independent noise logical failure probability due to data-qubits errors. The graph (a) plots the ratio against code distance for various p_z while (b) plots the ratio against p_z for selected code-distances *cd*

6.1 Logical failure probability trends in the noise sub-threshold region

The performance of surface code error correction is quantified by the fraction of incorrect decodings of error events due to (i) uncorrectable data-qubits errors (ii) faulty syndromes in the erroneous ancilla qubits. The correction procedure splits any arbitrary error event into sets of error which can be decoded into space and time separately [18]. The spatial-decoding, prescribed by the nearest-neighbors parity checks, determine the data-qubits errors, while temporal-decoding powered by repeated syndrome measurement identifies ancilla qubits errors. We leverage this bifurcation to partition our analysis into the logical failure incurred due to errors in data and ancilla qubits independently.

6.1.1 Logical failure probability due to data-qubits errors

The Figure-10 plots P_L against per-operation data qubit error probability for the selected code-distance $3 \leq cd \leq 19$. The curves converge at $p_z \approx P_L$ whereat threshold value: $p_{th} \approx 0.05$ falls within a factor of 3 of the previously known estimate [20]. In the sub-threshold region (i.e. $p_z \leq p_{th}$), the curves expectedly decay and diverge rapidly with the decreasing p_z and closely follow the known analytical expression $P_L \approx (\frac{p_z}{p_{th}})^{\frac{cd+1}{2}}$ [20] upto a small pre-factor. Overall, these trends can be closely compared with recent work on surface code fault-tolerant analysis [51].

In contrast, the correlated noise curves meeting at $p_{th} \approx 0.02$, *decay* and *diverge* contrastingly slower as they enter the sub-threshold region in Figure-11. Consequently, the ratio between correlated and independent P_L, (i.e. $\frac{P_L^{Corr}}{P_L^{Ind}}$) increases monotonically, not only with the decreasing p_z in Figure-12(b), but also with the increasing code-distance in Figure-12(a). The considerably higher P_L in case of the correlated noise can be generally explained using Figure-7, that error-correction fails to adequately curtail the logical errors resulting from the non-trivial probability $\Pr_{|k|}$ of many-qubit errors (i.e. larger $|k|$ values). Since considerable fraction ($f_{n,|k|} \approx 0.5$) of many-qubits errors remain uncorrectable, the exponentially higher $\Pr_{|k|}$ yields proportionally enlarged P_L. The increasing $\frac{P_L^{Corr}}{P_L^{Ind}}$ ratio can be explained by the expanding gap between correlated and independent curves shown in Figure-13. The increasing separation between the Figure-13(a) curves representing probability of many-qubits errors for the two noise models, indicates that $\frac{P_L^{Corr}}{P_L^{Ind}}$ ratio rises with the decreasing p_z. Similarly, a flatter tail logical failure probability trend is consistent with the exponentially increasing gap between the P_L curves in Figure-13(b) and confirms the analytically derived trends of P_L for the general CSS codes in Ref [32]. Our analysis shows that because logical failure probability cannot be efficiently lowered by increasing code distance only, the quantum threshold theorem no longer remains directly applicable to the correlated noise.

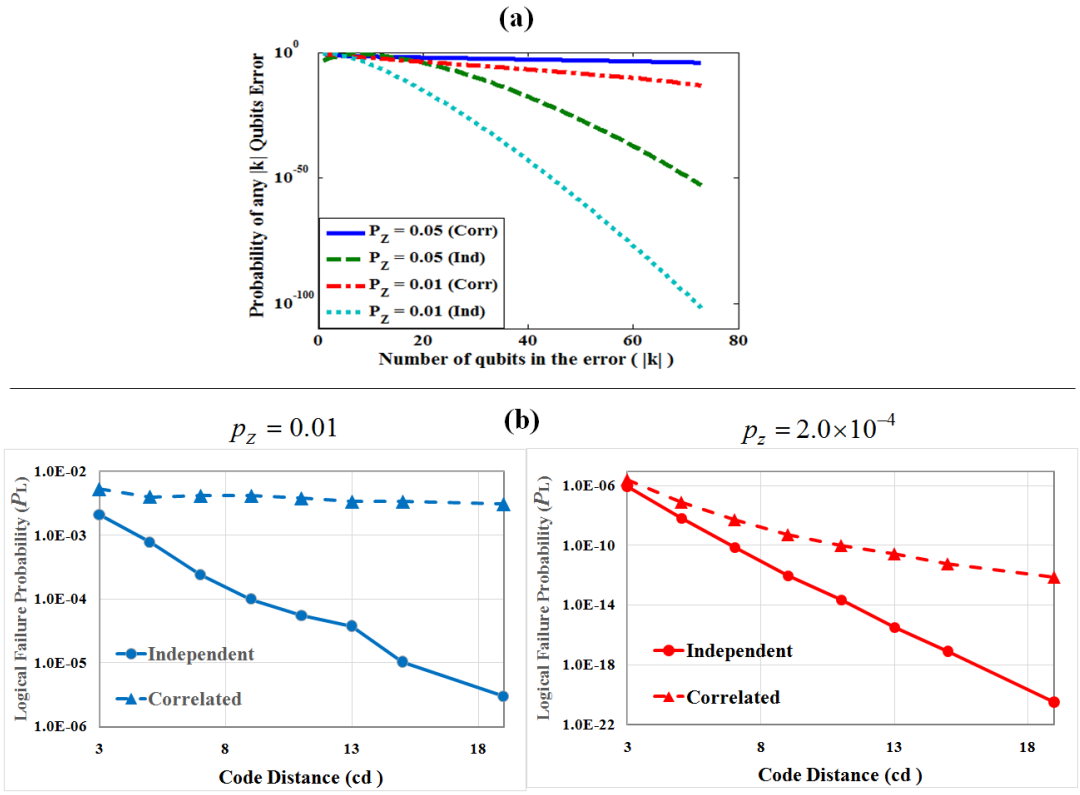

Figure 13: (Color online) In graph (a) $\Pr_{|k|}$ plotted against $|k|$ shows increasing gap between the correlated and independent data-qubits noise curves for two different p_z values. The gap explains the behavior of corresponding P_L curves in the Figure-12(a). In graph (b), P_L plotted against the code distance for $p_z = 0.01$ and $p_z = 2 \times 10^{-4}$. The expanding divergence between the curves of two types of noise explains Figure-12(b)

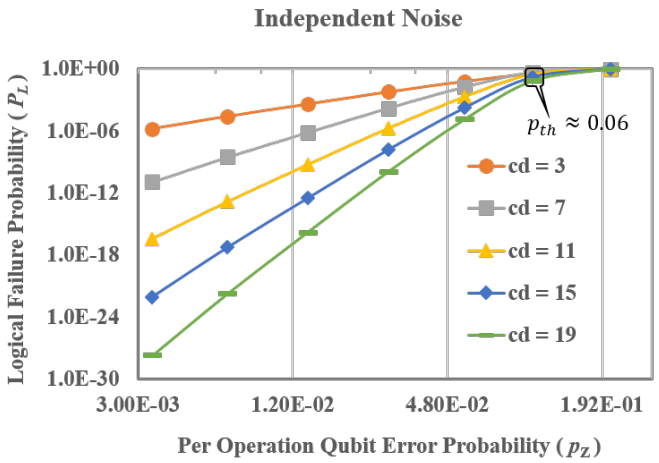

Figure 14: (Color online) The logical failure probability due to independent ancilla-qubits errors, plotted against per-operation qubit error probability for increasing code-distances *cd*

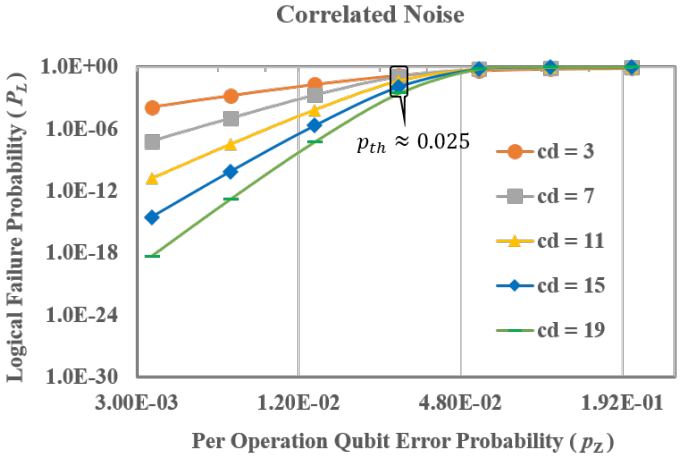

Figure 15: (Color online) The logical failure probability due to correlated ancilla-qubits errors, plotted against per-operation qubit error probability for increasing code-distances *cd*

6.1.2 Logical failure probability due to ancilla-qubits errors

The error correction procedure also fails due to faulty syndrome caused by ancilla qubits errors. As before, when the P_L curves for the two noise models are mutually contrasted (Figure-14 versus Figure-15), we find that the ancilla curves decline slowly but diverge rapidly in the presence of correlated noise. As a result, while the $\frac{P_L^{Corr}}{P_L^{Ind}}$ ratio rises exponentially with the code distance (similar to the case of data qubits) in Figure-16(a), it slowly increases and eventually flattens out at higher p_z as shown in Figure-16(b). The flattening behavior can be explained by analyzing ancilla qubit error probability in each trial of syndrome extraction whose duration is equal to the environment memory span. During each trial, the three sequential operations cause ancilla-qubits thrice interact the same environment and induce temporal noise correlation. According to Figure-4, the temporal noise correlation quadratically degrade fidelity of qubit which explains higher probability of error in the ancilla qubit. Table-1 lists the probability of ancilla error in each of the three trials of syndrome measurement for different p_z. The ratio between the ancilla error probabilities for the correlated and independent noise remains bounded and approaches constant value, so does the ratio $\frac{P_L^{Corr}}{P_L^{Ind}}$.

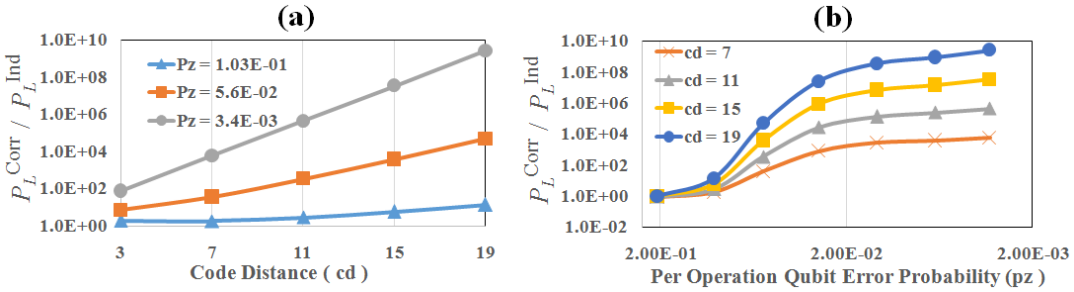

Figure 16: (Color online) The ratio between correlated and independent noise logical failure probability due to ancilla-qubits errors. The graph (a) plots the ratio against code distance for various p_z while (b) plots the ratio against p_z for selected code-distances cd

6.2 Reducing logical failure probability in correlated noise model

The comparison of Figures-11 and Figure-15 clearly reveals that data qubits errors define the performance bottleneck of quantum error correction. Due to the limited applicability of threshold theorem in our correlated noise model, the performance cannot be appreciably recuperated by increasing the code distance unless p_z is also curtailed.

Table 1: The ratio between the correlated and the independent noise logical failure probability due to ancilla-qubits errors, is listed against per-operation qubit failure probability (p_z). With decreasing p_z, the increase in the ratio gradually declines and eventually saturates to a value just above 3. This explains the trends of Figure-16(b)

	Per Operation Ancilla Qubit Failure Probability	Probability of Ancilla Error per Syndrome Extraction Trial		
		Independent Noise	Correlated Noise	Ratio: $\frac{\text{Correlated Noise}}{\text{Independent Noise}}$
1	**2.08 x 10^{-1}**	**4.0 x 10^{-1}**	**4.96 x 10^{-1}**	**1.24**
2	**1.03 x 10^{-1}**	**2.5 x 10^{-1}**	**4.37 x 10^{-1}**	**1.75**
3	**5.6 x 10^{-2}**	**1.5 x 10^{-1}**	**3.28 x 10^{-1}**	**2.19**
4	**2.82 x 10^{-2}**	**8 x 10^{-2}**	**2.04 x 10^{-1}**	**2.54**
5	**1.37 x 10^{-2}**	**4 x 10^{-2}**	**1.11 x 10^{-1}**	**2.77**
6	**6.68 x 10^{-3}**	**2 x 10^{-2}**	**5.7 x 10^{-2}**	**2.85**
7	**3.4 x 10^{-3}**	**1 x 10^{-2}**	**2.98 x 10^{-2}**	**2.98**
8	**1.7 x 10^{-3}**	**5 x 10^{-3}**	**1.51 x 10^{-2}**	**3.02**

If p_Z^{CORR} and p_Z^{IND} denote per- operation qubit error probability for correlated and independent noise respectively, then we can define factor $R := \frac{p_Z^{IND}}{p_Z^{CORR}}$ by which correlated p_z must to be reduced in order to achieve P_L on par with that achievable in the independent noise model. In the latter case, $P_L \leq 10^{-15}$ has shown to be sufficiently low to allow the reliable execution of large-scale quantum algorithms [3] (e.g. 1,024 bits integer factorization). Thus, if we wish to obtain the same P_L in correlated model, the factor R provides the desired reduction in p_Z^{CORR}. For $P_L \approx 10^{-15}$, the Figure-17 plots p_Z^{CORR}, p_Z^{IND} (left vertical axis) R (right vertical axis) for increasing code distances. The dark black line necessitates R increases linearly, thus, p_z should decrease linearly with the code-distance.

Since the linear increase in the code distance amounts to the quadratic raise in the number of data-qubits n comprising surface code logical qubit, the curve bends sub-linearly when R is plotted against n. The Figure-18 plots three prominently overlapping curves, for each of the $P_L = 10^{-15}, 10^{-20}$ and 10^{-25}. We find that the function $R = 0.28n^{0.49} + 0.73$ grows slightly faster than the curve for $P_L = 10^{-15}$ but closely fits to the curves for $P_L = 10^{-20}$ and 10^{-25}. Since R increases no faster than $n^{0.5}$, therefore, once the code distance is selected to achieve target P_L with p_Z^{IND}, the presence of noise correlation stipulates that $p_Z^{CORR} = O(\frac{1}{\sqrt{n}})p_Z^{IND}$. Thus, per-operation qubit error probability may be reduced by the factor $O(\sqrt{n})$ for correlated noise model if we wish to accomplish progressively lower logical failure probability.

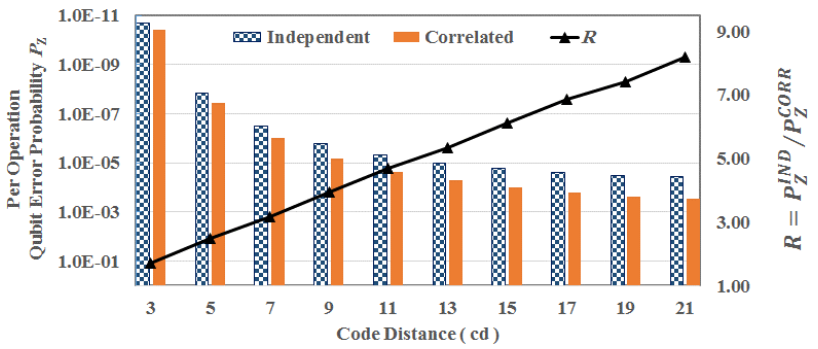

Figure 17: (Color online) The p_z required to achieve $P_L \approx 10^{-15}$ is plotted against code-distance on left vertical axis for both independent and correlated noise models. The Failure Probability Ratio R between independent p_z (denoted as p_z^{IND}) and correlated p_z (denoted as p_z^{CORR}) is plotted against code-distance on the right vertical axis

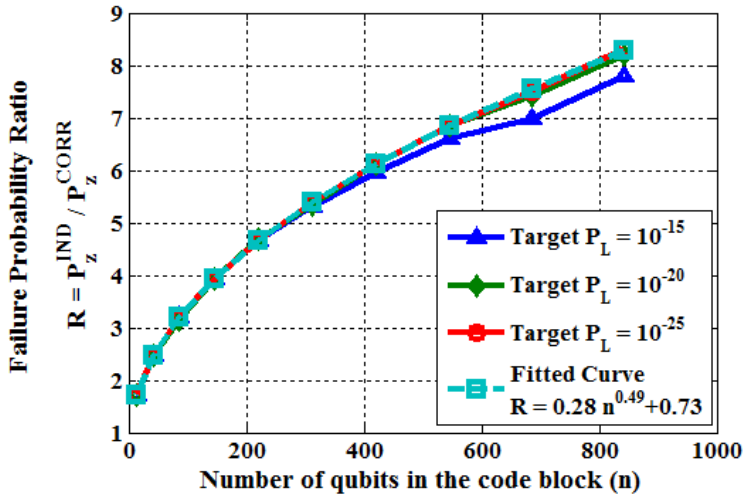

Figure 18: (Color online) For various target P_L, the Failure Probability Ratio R is plotted against n: the number of data-qubits in the surface error correcting codeword. The fitted curve shows that R approximately increases as $n^{0.5}$ which shows that correlated noise p_z may be reduced by factor $\sqrt{n}$ in order to match the performance of independent noise

7 Discussion

Our $O(\sqrt{n})$ result denies the foundational advantage promised by the Quantum Threshold Theorem [1, 5]; that the constant noise level below certain threshold suffices both fault-tolerant and scalable computation while incurring modest resources overhead. However, in order to obtain deeper insight into the consequence of this result, we carefully parse threshold theorem along the following interpretation of *fault-tolerance* and *scalability*. A quantum circuit is said to be fault-tolerantly executed when logical failure probability reduces to arbitrarily low value with constant noise level per operation. This is different from scalability which primarily seeks acceptable scaling of codeword qubits (resource overhead) to achieve progressively lower logical failure probability. This bifurcation motivated us to distinguish between the logical failure probability P_L curves (2-D Figures-10 through 16) plotted with respect to p_z and those graphed against cd.

We used independent noise model as benchmark case which enabled surface error correcting code to achieve both fault-tolerance and scalability [18]. This was validated by the P_L decreasing (i) super exponentially with respect to p_z (Figure-10) and (ii) exponentially decreasing with cd (**Ind** curves in Figure-13(b)). These trends (consistent with the prior works on surface code fault-tolerance, see Section-6) set benchmark of fault-tolerance and scalability for the correlated noise model. However, we noted that P_L declined sub-exponentially with both p_z (Figure-11) and cd (**Corr** curves in Figure-13(b)) in the correlated model. In the latter plot, we noted that P_L became nearly flat with cd indicating that resource overhead would not benefit appreciable reduction in P_L unless p_z was also reduced proportionally. This asymptotic flatness may also be validated analytically [32] using (5) and (8). We note that logical failure occurs when number of errors ($|k|$ in (5)) exceed $d = \frac{cd+1}{2}$. Thus P_L can be expressed as $\sum_{|k|=d}^{n} f_{n,|k|}\mathrm{Pr}_k$.The Figure-7 shows that $f_{n,|k|}$ gradually saturates to 0.5 and that is generally true also for all cd considered in this work. Therefore, by letting $f_{n,|k|} = 0.5$ and commuting summation inside integral of (5), we obtain

$$P_L \approx \frac{1}{2\sqrt{\pi L_d}} \int_{-\infty}^{\infty} e^{-\frac{z^2}{L_d}} \sum_{|k|=d}^{n} \binom{n}{|k|} \tilde{p}_z^{|k|}(1-\tilde{p}_z)^{n-|k|} dz$$

In the limit $n \longrightarrow \infty$, the component of summation approaches 0 for $\tilde{p}_z < d/n$, while it converges to 1 when $\tilde{p}_z \geq d/n$ [32]. After simplification, we find that

$$P_L \approx \frac{1}{2\sqrt{\pi L_d}} \int_{\tilde{p}_z \geq d/n} e^{-\frac{z^2}{L_d}} dz$$

In the sub-threshold region, the variance L_d, of zero-mean normal random variable z, is small, then $\tilde{p}_z = \frac{1-\cos(2z)}{2} = \sin^2(z) \approx z^2$. The integral limits can then be

transformed into $|z| \geq \sqrt{d/n}$. Hence we obtain following P_L expression:

$$P_L \approx \frac{1}{\sqrt{\pi L_d}} \int_{|z| \geq \sqrt{d/n}} e^{-\frac{z^2}{L_d}} dz = \text{erfc}(\sqrt{\frac{d}{nL_d}}) \tag{9}$$

The (9) shows that P_L approaches non-trivial constant $\sim \text{erfc}(\sqrt{\frac{d}{nL_d}})$ when $n \longrightarrow \infty$.

Since increasing surface code size failed to sufficiently attenuate P_L, we proposed *conditional scalability criterion* based on lowering correlation strength L_d indirectly by reducing p_z. Thus, in order for correlated noise to achieve some low target P_L which the benchmark noise achieves with efficient resource scaling, we defined ratio: R as the factor by which correlated p_z should be reduced (compared to the corresponding p_z in independent noise) to achieve target P_L for given cd. The dark black line in Figure-17 described linear relationship between R and cd, while Figure-18 showed that R increased $O(\sqrt{n})$ against the size n (number of qubits in the) codeword for each progressively smaller value of P_L: (10^{-15}, 10^{-20} and 10^{-25}). Hence we required p_z scale down $O(\sqrt{\text{size of codeword}})$ times below the threshold to achieve arbitrarily low P_L. These results are summarized as follows:

1. Our *conditional scalability* criterion requires that correlated noise model has same logical failure probability as that of independent noise model, for given code distance.

2. For given size n of surface error correcting codeword, the logical failure probability in case of correlated noise model can match that of the benchmark noise model for the same code distance, provided that noise level per-operation is also reduced by the factor $O(\sqrt{n})$ in the sub-threshold region. However, this result on conditional scalability assumes maximal noise correlation strength.

3. Since code distance remains same in both the models, the error-correction in correlated model does not incur surplus resource overhead compared to the benchmark noise model.

4. If the decreasing noise level condition is met, then according to the aforementioned interpretation, we can say that conditional scalability can be achieved by the correlated noise.

5. On contrary, the condition of decreasing physical noise levels in sub-threshold region, clearly denies fault-tolerance in case of correlated noise.

These results hint at redirecting ongoing experimental efforts rooted in the premise that larger and more reliable quantum computers can be built with each of its component qubit or gate failing with some fixed probability below certain threshold. This prevalent belief is founded on the assumption that failure of components bear no mutual correlation i.e. each component fails independently. Recent advancements in the

characterization of noise in real quantum hardware have established noise correlations and invalidate independent failure assumption. Given that the noise in realistic quantum hardware may have correlated nature as proposed and evaluated in this work, experimentalists should not expect to achieve scalability only through the integration of more components whose failure probability is upper bounded by some constant accuracy threshold. Instead, they should also strive for increasing noise margin; by reducing failure probability as far below the accuracy threshold as possible.

8 Conclusion

In this study, we proposed and presented quantum circuit based intuitive snapshot of a more realistic correlated noise model which decoheres the qubits by coupling them to the same environment. The model was parametrized by the strength of noise correlation as well as short-term memory and long-range spatial correlations. We leveraged prior studies to interpret the physical significance of our model parameters and highlighted their role in testing the efficacy of the structure of surface code error correction scheme. We investigated the detrimental effects of noise correlation on the performance of the error-correction by comparing it with the independent noise case. We showed that the likelihood of error correction failure was significantly higher and evidently deviated from the trends anticipated by the quantum threshold theorem primarily proposed for the independent noise model. The overall statistical error in the data was confined to acceptable limits, validating our simulation results within 95% confidence interval.

The insightful performance comparison was facilitated by efficient computation of error probability distribution and single scale for measuring the strength of both types of noise. The scale quantified the qubit error probability resulting from each gate operation and became a crucial scalable design constraint of the fault-tolerant quantum computation. We concluded our analysis by showing that increasing code-distance did not yield desired level of logical failure probability unless per-operation qubit error probability was also concurrently reduced.

9 Acknowledgements

We would like to thank Rochus Klesse, Jungsang Kim and Rodney Van Meter for the helpful discussions and critical reading of the manuscript.

References

[1] Dorit Aharonov and Michael Ben-Or. Fault-tolerant quantum computation with constant error. In *Proceedings of the twenty-ninth annual ACM symposium on Theory of computing*, pages 176–188. ACM, 1997.

[2] Dorit Aharonov, Alexei Kitaev, and John Preskill. Fault-tolerant quantum computation with long-range correlated noise. *Physical review letters*, 96(5):050504, 2006.

[3] Muhammad Ahsan, Rodney Van Meter, and Jungsang Kim. Designing a million-qubit quantum computer using a resource performance simulator. *ACM Journal on Emerging Technologies in Computing Systems (JETC)*, 12(4):39, 2016.

[4] Robert Alicki. Quantum error correction fails for hamiltonian models. *Fluctuation and Noise Letters*, 6(03):C23–C28, 2006.

[5] Panos Aliferis, Daniel Gottesman, and John Preskill. Quantum accuracy threshold for concatenated distance-3 codes. *arXiv preprint quant-ph/0504218*, 2005.

[6] Dave Bacon. Operator quantum error-correcting subsystems for self-correcting quantum memories. *Physical Review A*, 73(1):012340, 2006.

[7] Avraham Ben-Aroya and Amnon Ta-Shma. Approximate quantum error correction for correlated noise. *IEEE Transactions on Information Theory*, 57(6):3982–3988, 2011.

[8] Nadja K Bernardes, Alvaro Cuevas, Adeline Orieux, CH Monken, Paolo Mataloni, Fabio Sciarrino, and Marcelo F Santos. Experimental observation of weak non-markovianity. *Scientific reports*, 5:17520, 2015.

[9] Sergey B Bravyi and A Yu Kitaev. Quantum codes on a lattice with boundary. *arXiv preprint quant-ph/9811052*, 1998.

[10] Heinz-Peter Breuer, Elsi-Mari Laine, and Jyrki Piilo. Measure for the degree of non-markovian behavior of quantum processes in open systems. *Physical review letters*, 103(21):210401, 2009.

[11] Heinz-Peter Breuer, Elsi-Mari Laine, Jyrki Piilo, and Bassano Vacchini. Colloquium: Non-markovian dynamics in open quantum systems. *Reviews of Modern Physics*, 88(2):021002, 2016.

[12] A Robert Calderbank and Peter W Shor. Good quantum error-correcting codes exist. *Physical Review A*, 54(2):1098, 1996.

[13] Andrea Chiuri, Chiara Greganti, Laura Mazzola, Mauro Paternostro, and Paolo Mataloni. Linear optics simulation of quantum non-markovian dynamics. *Scientific reports*, 2:968, 2012.

[14] Eric Dennis, Alexei Kitaev, Andrew Landahl, and John Preskill. Topological quantum memory. *Journal of Mathematical Physics*, 43(9):4452–4505, 2002.

[15] Simon J Devitt. Performing quantum computing experiments in the cloud. *Physical Review A*, 94(3):032329, 2016.

[16] Lu-Ming Duan and Guang-Can Guo. Reducing decoherence in quantum-computer memory with all quantum bits coupling to the same environment. *Physical Review A*, 57(2):737, 1998.

[17] Felipe F Fanchini, Goktug Karpat, Baris Çakmak, LK Castelano, GH Aguilar, O Jiménez Farías, SP Walborn, PH Souto Ribeiro, and MC De Oliveira. Non-markovianity through accessible information. *Physical Review Letters*, 112(21):210402, 2014.

[18] Austin G Fowler. Analytic asymptotic performance of topological codes. *Physical Review A*, 87(4):040301, 2013.

[19] Austin G Fowler. Minimum weight perfect matching of fault-tolerant topological quantum error correction in average $o(1)$ parallel time. *arXiv preprint arXiv:1307.1740*, 2013.

[20] Austin G Fowler, Matteo Mariantoni, John M Martinis, and Andrew N Cleland. Surface codes: Towards practical large-scale quantum computation. *Physical Review A*, 86(3):032324, 2012.

[21] Jay M Gambetta, Jerry M Chow, and Matthias Steffen. Building logical qubits in a superconducting quantum computing system. *arXiv preprint arXiv:1510.04375*, 2015.

[22] Crispin Gardiner and Peter Zoller. *Quantum noise: a handbook of Markovian and non-Markovian quantum stochastic methods with applications to quantum optics*, volume 56. Springer Science & Business Media, 2004.

[23] Crispin W Gardiner and Hermann Haken. *Quantum noise*, volume 26. Springer Berlin, 1991.

[24] TP Harty, DTC Allcock, C J Ballance, L Guidoni, HA Janacek, NM Linke, DN Stacey, and DM Lucas. High-fidelity preparation, gates, memory, and readout of a trapped-ion quantum bit. *Physical review letters*, 113(22):220501, 2014.

[25] Jiasen Jin, Vittorio Giovannetti, Rosario Fazio, Fabio Sciarrino, Paolo Mataloni, Andrea Crespi, and Roberto Osellame. All-optical non-markovian stroboscopic quantum simulator. *Physical Review A*, 91(1):012122, 2015.

[26] Gil Kalai. How can quantum computers fail? Technical report, 2006.

[27] Gil Kalai. Detrimental decoherence. *arXiv preprint arXiv:0806.2443*, 2008.

[28] Gil Kalai. Quantum computers: noise propagation and adversarial noise models. *arXiv preprint arXiv:0904.3265*, 2009.

[29] Alastair Kay and Jiannis K Pachos. Quantum computation in optical lattices via global laser addressing. *New Journal of Physics*, 6(1):126, 2004.

[30] Jungsang Kim. Trapped ions make impeccable qubits. *Physics*, 7:119, 2014.

[31] A Yu Kitaev. Fault-tolerant quantum computation by anyons. *Annals of Physics*, 303(1):2–30, 2003.

[32] Rochus Klesse and Sandra Frank. Quantum error correction in spatially correlated quantum noise. *Physical review letters*, 95(23):230503, 2005.

[33] Emanuel Knill. Quantum computing with very noisy devices. *arXiv preprint quant-ph/0410199*, 2004.

[34] Elsi-Mari Laine, Jyrki Piilo, and Heinz-Peter Breuer. Measure for the non-markovianity of quantum processes. *Physical Review A*, 81(6):062115, 2010.

[35] Andrew J Landahl, Jonas T Anderson, and Patrick R Rice. Fault-tolerant quantum computing with color codes. *arXiv preprint arXiv:1108.5738*, 2011.

[36] Daniel A Lidar and Todd A Brun. *Quantum error correction*. Cambridge University Press, 2013.

[37] Bi-Heng Liu, Dong-Yang Cao, Yun-Feng Huang, Chuan-Feng Li, Guang-Can Guo, Elsi-Mari Laine, Heinz-Peter Breuer, and Jyrki Piilo. Photonic realization of nonlocal memory effects and non-markovian quantum probes. *Scientific reports*, 3:1781, 2013.

[38] Bi-Heng Liu, Li Li, Yun-Feng Huang, Chuan-Feng Li, Guang-Can Guo, Elsi-Mari Laine, Heinz-Peter Breuer, and Jyrki Piilo. Experimental control of the transition from markovian to non-markovian dynamics of open quantum systems. *Nature Physics*, 7(12):931, 2011.

[39] DH Mahler, Lee A Rozema, Ardavan Darabi, Christopher Ferrie, Robin Blume-Kohout, and AM Steinberg. Adaptive quantum state tomography improves accuracy quadratically. *Physical review letters*, 111(18):183601, 2013.

[40] Ari Mizel and Daniel A. Lidar. Exchange interaction between three and four coupled quantum dots: Theory and applications to quantum computing. *Phys. Rev. B*, 70:115310, Sep 2004.

[41] Eduardo Novais and Harold U Baranger. Decoherence by correlated noise and quantum error correction. *Physical review letters*, 97(4):040501, 2006.

[42] G Massimo Palma, Kalle-Antti Suominen, and Artur K Ekert. Quantum computers and dissipation. In *Proceedings of the Royal Society of London A: Mathematical, Physical and Engineering Sciences*, volume 452, pages 567–584. The Royal Society, 1996.

[43] Martin B Plenio, Vlatko Vedral, and Peter L Knight. Quantum error correction in the presence of spontaneous emission. *Physical Review A*, 55(1):67, 1997.

[44] John Preskill. Sufficient condition on noise correlations for scalable quantum computing. *arXiv preprint arXiv:1207.6131*, 2012.

[45] Robert Raussendorf and Jim Harrington. Fault-tolerant quantum computation with high threshold in two dimensions. *Physical review letters*, 98(19):190504, 2007.

[46] A Shabani. Correlated errors can lead to better performance of quantum codes. *Physical Review A*, 77(2):022323, 2008.

[47] K. Shiokawa and D. A. Lidar. Dynamical decoupling using slow pulses: Efficient suppression of $1/f$ noise. *Phys. Rev. A*, 69:030302, Mar 2004.

[48] Peter W. Shor. Scheme for reducing decoherence in quantum computer memory. *Phys. Rev. A*, 52:R2493–R2496, Oct 1995.

[49] Daan Staudt. The role of correlated noise in quantum computing. *arXiv preprint arXiv:1111.1417*, 2011.

[50] Andrew Steane. Multiple-particle interference and quantum error correction. In *Proceedings of the Royal Society of London A: Mathematical, Physical and Engineering Sciences*, volume 452, pages 2551–2577. The Royal Society, 1996.

[51] Ashley M Stephens. Fault-tolerant thresholds for quantum error correction with the surface code. *Physical Review A*, 89(2):022321, 2014.

[52] Jian-Shun Tang, Chuan-Feng Li, Yu-Long Li, Xu-Bo Zou, Guang-Can Guo, Heinz-Peter Breuer, Elsi-Mari Laine, and Jyrki Piilo. Measuring non-markovianity of processes with controllable system-environment interaction. *EPL (Europhysics Letters)*, 97(1):10002, 2012.

[53] Barbara M Terhal. Quantum error correction for quantum memories. *Reviews of Modern Physics*, 87(2):307, 2015.

[54] Barbara M Terhal and Guido Burkard. Fault-tolerant quantum computation for local non-markovian noise. *Physical Review A*, 71(1):012336, 2005.

[55] Rodney Van Meter and Clare Horsman. A blueprint for building a quantum computer. *Communications of the ACM*, 56(10):84–93, 2013.

[56] Giovanni Viola and Gianluigi Catelani. Collective modes in the fluxonium qubit. *Phys. Rev. B*, 92:224511, Dec 2015.

[57] Lorenza Viola and Seth Lloyd. Dynamical suppression of decoherence in two-state quantum systems. *Phys. Rev. A*, 58:2733–2744, Oct 1998.

[58] Tao Xin, Dawei Lu, Joel Klassen, Nengkun Yu, Zhengfeng Ji, Jianxin Chen, Xian Ma, Guilu Long, Bei Zeng, and Raymond Laflamme. Quantum state tomography via reduced density matrices. *Physical Review Letters*, 118(2):020401, 2017.